Tsunami Forecast by Joint Inversion of Real-Time Tsunami Waveforms and Seismic or GPS Data: Application to the Tohoku 2011 Tsunami

YONG WEI,[1,2] ANDREW V. NEWMAN,[3] GAVIN P. HAYES,[4] VASILY V. TITOV,[1] and LIUJUAN TANG[1,2]

Abstract—Correctly characterizing tsunami source generation is the most critical component of modern tsunami forecasting. Although difficult to quantify directly, a tsunami source can be modeled via different methods using a variety of measurements from deep-ocean tsunameters, seismometers, GPS, and other advanced instruments, some of which in or near real time. Here we assess the performance of different source models for the destructive 11 March 2011 Japan tsunami using model–data comparison for the generation, propagation, and inundation in the near field of Japan. This comparative study of tsunami source models addresses the advantages and limitations of different real-time measurements with potential use in early tsunami warning in the near and far field. The study highlights the critical role of deep-ocean tsunami measurements and rapid validation of the approximate tsunami source for high-quality forecasting. We show that these tsunami measurements are compatible with other real-time geodetic data, and may provide more insightful understanding of tsunami generation from earthquakes, as well as from nonseismic processes such as submarine landslide failures.

Key words: Tsunameter, GPS, finite-fault solution, tsunami, inversion, tsunami forecast, runup, inundation, modeling, near field.

1. Introduction

Rapid seafloor deformation caused by earthquake slip is the dominant source of large long-wavelength transoceanic waves driven by gravity, termed tsunami. Determination of tsunami source characteristics in the early stages of a progressing tsunami is crucial for accurate and useful inundation and runup forecasting. At present, deep-ocean tsunameters, seismographic networks, and high-rate GPS stations are probably the most capable instruments for providing real-time observations of earthquake rupture and tsunami propagation. These observations can be used for rapid estimation of a slip-distribution-based tsunami source, which can in turn be used as direct input for model forecasts of tsunami impact in real time (TANG *et al.*, 2012; WEI *et al.*, 2013) or near real time (HAYES *et al.*, 2011).

A tsunami source, for which the water column is instantaneously disturbed by the deformed ocean bottom, can be inferred from a variety of tsunami measurements provided by deep-ocean tsunameters (WEI *et al.*, 2003, 2008; TITOV *et al.*, 2005; TITOV, 2009; PERCIVAL *et al.*, 2010), cabled ocean-bottom pressure sensors (TSUSHIMA *et al.*, 2009), satellite altimetry (ARCAS and TITOV, 2006; HIRATA *et al.*, 2006), and/or tide gage data (SATAKE, 1987; SATAKE and KANAMORI, 1991). An indirect measure of a tsunami source can come from the estimation of coseismic displacements resulting from fault slip, assuming that the resulting vertical disturbance of the ocean floor is instantaneously transferred to the ocean surface (KAJIURA, 1970). Traditionally, the approximate location, depth, fault orientation, and seismic moment of an event can be approximated from a centroid moment tensor (CMT) solution within 8–15 min after large earthquakes (WHITMORE, 2009). However, since they assume a point source, CMT inversions do not adequately describe the spatial extent of rupture, causing tsunami forecasts to be inaccurate for coastal communities at risk (GOVERNMENT ACCOUNTABILITY OFFICE, 2006). In the last decade, finite-fault inversion algorithms using globally distributed broadband seismic waveforms have

---

[1] Joint Institute for the Study of the Atmosphere and Ocean, University of Washington, Seattle, WA, USA. E-mail: Yong.Wei@noaa.gov

[2] Pacific Marine Environmental Laboratory, National Oceanic and Atmospheric Administration, Seattle, WA, USA.

[3] School of Earth and Atmospheric Sciences, Georgia Institute of Technology, Atlanta, GA, USA.

[4] United States Geological Survey, National Earthquake Information Center, Golden, Colorado, USA.

become a widely used technique to constrain the detailed spatial dimensions and slip distribution of the seismic source (hereafter "earthquake source dimensions"; e.g., Ji et al., 2002). This methodology has been used as source input for models of tsunami from some recent large earthquakes (Fritz et al., 2011; Newman et al., 2011; Yamazaki et al., 2011; Wei et al., 2013; MacInnes et al., 2013). Global Positioning System (GPS) data offer precise measurements of ground displacements from an earthquake rupture, which have been shown to facilitate computation of earthquake slip parameters shortly after large events (Blewitt et al., 2006; Pietrzek et al., 2007; Simons et al., 2011; Vingy et al., 2011; Song et al., 2012).

Each method has its own merits and limitations. Tsunameters provide direct measurements of the water pressure changes caused by tsunami waves, which are in general the earliest direct tsunami observations available during an event. Different from the water level registered at tide gages, deep-ocean tsunami data are free of interference from harbor and local shelf effects, yet are not sensitive to short-wavelength wind-driven waves, leaving clean signatures (resolution to the sub-cm level) of the tsunami. Because tsunami propagation in the deep ocean follows linear wave dynamics, pressure information from tsunameters allows for rapid tsunami source inversions (Satake, 1987; Satake and Kanamori, 1991; Wei et al., 2003; Percival et al., 2010). Real-time tsunami measurements in the deep ocean are the core component of the NOAA's tsunami forecast system, and have led to many successful real-time forecasts in the last decade, especially after the 2004 Indian Ocean tsunami (González et al., 2005; Titov, 2009; Tang et al., 2008, 2012; Wei et al., 2008, 2013). Tsunameters are predominantly sited near subduction zones—the environment responsible for most tsunamigenic earthquakes. Instruments are placed at distances equivalent to 30–60 min of tsunami wave travel time from expected tsunamigenic earthquake sources, and seaward of the trench to avoid effects from coastal and shallow-water interference that complicate signals by causing nonlinearity and dispersion of waves (Spillane et al., 2008). Unfortunately, such tsunameter data are particularly critical in the first 30 min for near-field

tsunami warning and forecasting. Several, more proximal tsunameters were recently deployed offshore of Japan and provided useful data within 10–20 min after the 7 December 2012 moment magnitude (M_w) 7.2 Japanese earthquake, which generated a small tsunami (Bernard et al., 2013). This improvement shows that tsunami detection times can be significantly shortened when tsunameters are located closer to potential sources (Wei et al., 2013).

Inversion of seismic waves via finite-fault modeling is a method used to rapidly characterize an earthquake source in terms of its spatiotemporal slip distribution (Ji et al., 2002; Hayes, 2011, and references therein). Following the 2011 Japan earthquake, the US Geological Survey (USGS) National Earthquake Information Center (NEIC) provided a quick finite slip model within several hours of the earthquake origin time (Hayes, 2011). This method is robust for capturing the broad characteristics of an earthquake's slip distribution, but can be limited by the initial assumption of the fault geometry (Hayes, 2011). For tsunami modeling, a major concern when using such fault slip models is that the energy conversion process—from fault rupture to ocean water—remains one of the most difficult geophysical problems to solve. For great earthquakes, such as the 2004 Sumatra, Indonesia and 2011 Tohoku-Oki, Japan events, one of the biggest challenges is to quickly determine an accurate magnitude for the earthquake, since the time available for analysis of the energy content in long-period seismic waves is limited to before waves arrive at the closest shorelines (Whitmore, 2009). In the past, moment variations have been as large as a factor of ten between initial and final estimations (Tang et al., 2012). In the future, analyses of the seismic W-phase (Duputel et al., 2012), particularly at regional distances (Rivera et al., 2011), will help to improve both the accuracy and speed of rapid magnitude estimates.

Ground deformation monitors such as GPS provide accurate measurements of fault movement that can be used to reconstruct the detailed structure of the earthquake source. However, except for a very few underwater measurements during the Tohoku earthquake (Sato et al., 2011), which were not available in real time, GPS instruments are mostly tied to land-based observations because the radar signals used

cannot penetrate water, and thus the results are inadequate for characterizing earthquake slip that occurs predominantly offshore and near the trench, where it is most effective at tsunami generation (NEWMAN, 2011). Therefore, the exclusive use of land-based GPS measurements may lead to poorly constrained estimates of tsunami sources. One solution is to combine coseismic measurements made on land with deep-ocean tsunameter measurements. GUSMAN et al. (2010) performed a retrospective joint inversion of tsunami waveforms and InSAR data to understand the magnitude and spatial extent of the 2007 Bengkulu earthquake. YOKOTA et al. (2011) reassessed the 2011 Tohoku earthquake source via a joint inversion of strong motion, teleseismic, geodetic, and tsunami datasets. YAMAZAKI et al. (2011) applied a perturbation method to tune the tsunami model results using tsunami measurements to improve the finite-fault inversions.

The deadly 11 March 2011 Japan tsunami is likely the fourth largest documented in history from the perspective of tsunami energy (TANG et al., 2012). It is also the largest event to have been widely recorded by tsunameter, seismic, and GPS networks. Despite the early tsunami warning in Japan 3 min after the earthquake based on a preliminary magnitude of M_w 7.9 event (OZAKI, 2012), the earliest estimate of the tsunami source itself came from NOAA's inversion model using waveforms recorded at a tsunameter (also called DART® in the USA as an acronym for Deep-ocean Assessment and Reporting for Tsunamis) 500 km east of the epicenter about an hour after the earthquake (TANG et al., 2012; WEI et al., 2013). The earliest estimates of the earthquake source useful for tsunami modeling were the USGS CMT and rapid finite-fault model solutions (HAYES, 2011; HAYES et al., 2011), both inferred from seismological data within minutes to hours of the mainshock. GPS stations throughout Japan recorded measurements of coseismic offsets within minutes of the earthquake, and these measurements, if made available in real time, could have aided a very rapid estimate of earthquake source dimensions (OHTA et al., 2012).

In the following sections, we assess source models inferred from different real-time measurements for prediction of the 11 March 2011 Japan tsunami (Fig. 1). We use these source models as input for a

tsunami model, and compare the modeling results with real-time measurements and survey results for the 2011 Tohoku tsunami. This comparative study provides an overview of the advantages and limitations of different real-time measurements potentially useful for early tsunami warning in the near and far fields.

2. Methodology and Tsunami Models

In this study, we use the tsunami inundation models developed in WEI et al. (2013) to simulate the 2011 Tohoku tsunami for all source models. These inundation models are based on the Method of Splitting Tsunami (MOST), a suite of numerical simulation codes capable of estimating tsunami generation, transoceanic propagation, and inundation (TITOV et al., 1997; TITOV and SYNOLAKIS, 1998). MOST uses nonlinear shallow-water (NSW) equations with bottom friction and a moving boundary to compute the tsunami inundation on land. We note here that, in NSW, wave breaking manifests itself as a discontinuity of the solution (TITOV and SYNOLAKIS, 1998). Because mass and momentum are conserved in MOST, the computed solution reflects the overall evolution of tsunami inundation without reproducing the details of the breaking front. With proper setup between the spatial and temporal time steps, the MOST model can numerically mimic the physical wave dispersion (BURWELL et al., 2007). ZHOU et al. (2012) demonstrated that predictions generated using MOST, a shallow-water model with numerical dispersion, and a fully dispersive model developed by ZHOU et al. (2011) all perform comparably in predicting the leading waves of a tsunami. We note here that a two-dimensional (2D) shallow-water model with numerical dispersion such as MOST cannot fully reproduce the physical dispersion of a tsunami as a Boussinesq (dispersive NSW) model does (LOVHOLT et al., 2010). The most significant discrepancies exist in the short trailing waves, and may be more noticeable at distant destinations, during a dispersive tsunami (ZHOU et al. 2011). However, from the perspectives of runup/rundown, wave breaking, and computational efficiency, MOST is more robust, efficient, and flexible as a real-time computational
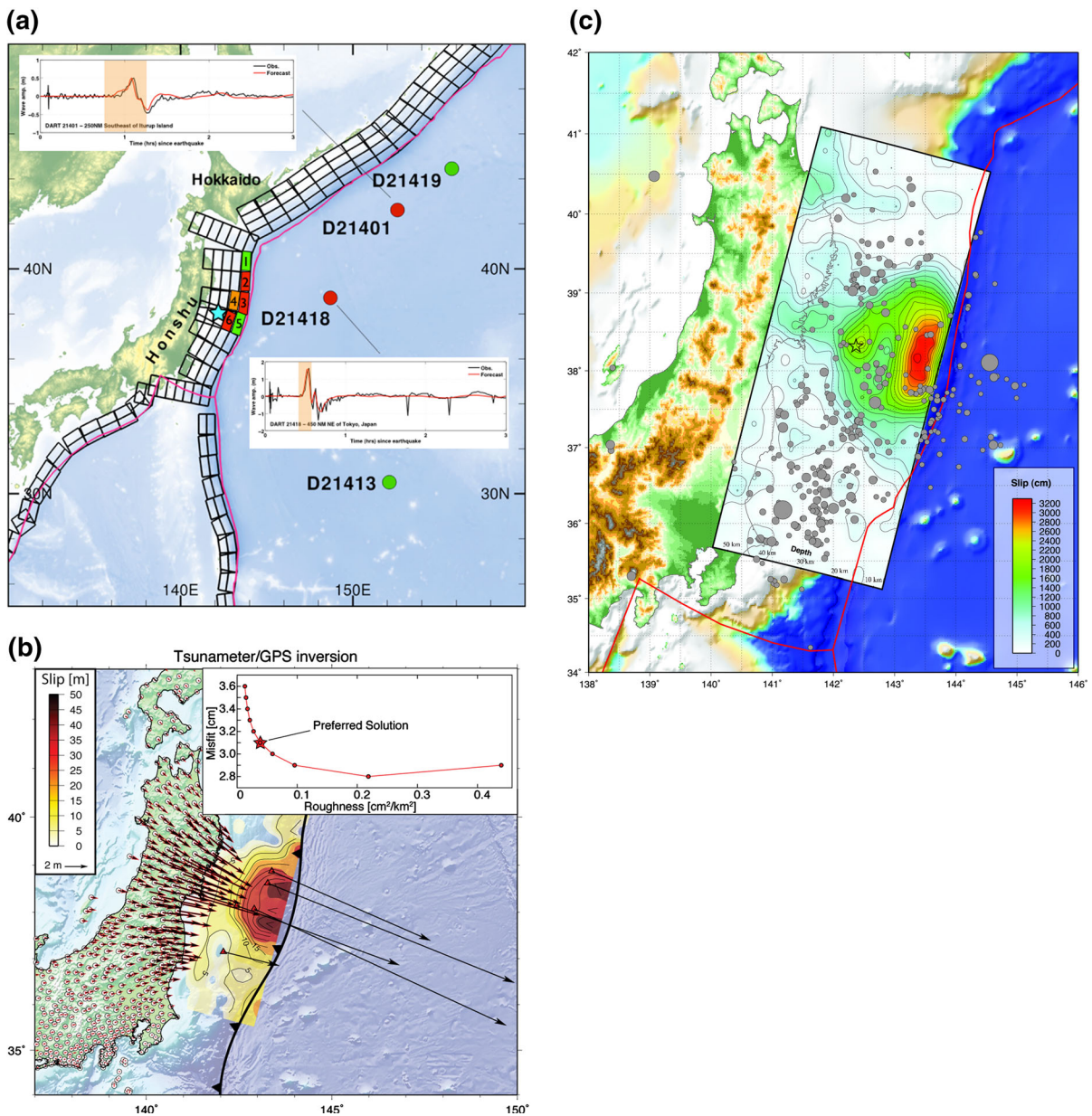
Figure 1

a The 11 March 2011 Japan tsunami source inferred from tsunameter measurements. This inversion was based on real-time measurements from tsunameters D21418 and D21401, where the *orange area* indicates the segment of the time series used in the inversion. The *cyan star* is the USGS epicenter for the 2011 Tohoku earthquake. The *purple line* indicates the plate boundaries. The *black boxes* are the 100 km × 50 km tsunami unit sources precomputed in NCTR's database. The *filled boxes* reflect the inversion results with *color* indicating the slip amount (details in Table 1). **b** GPS/tsunameter inversion for slip along a single 12° dipping plane (*color contours*). Onland GPS data (*black arrows*) are mimicked by the inversion prediction of ground displacement (*red arrows* behind). Seafloor horizontal displacements from SATO *et al.* (2011), which were not used in the inversion, are shown for comparison. An *inset* shows the relative trade-off between decreased roughness (increased smoothness) and misfit. The preferred slip solution is chosen near an inflection point where further reductions in model roughness significantly increase misfit. **c** Surface projection of the slip distribution superimposed on GEBCO bathymetry. *Red lines* indicate major plate boundaries (BIRD, 2003). *Gray circles*, if present, are aftershock locations, sized by magnitude (http://earthquake.usgs.gov/earthquakes/eqinthenews/2011/usc0001xgp/finite_fault.php)

tool compared with a fully dispersive model (Lov-holt *et al.*, 2010). MOST employs the elastic model of Okada (1985) to compute the initial seafloor deformation resulting from a source model, predictions that are then used directly as the initial deformation of the ocean surface in the tsunami inundation models (Kajiura, 1970). The MOST model has been tested against laboratory experiments and benchmarks (Synolakis *et al.*, 2008). Since the 2004 Indian Ocean tsunami, MOST has been validated against many modern tsunamis, and used to forecast the tsunami waves at many harbors along US coastlines.

MacInnes *et al.* (2013) used tsunami inundation models to evaluate source dimensions for nine earthquakes solely or jointly from tsunami measurements, seismic data, and GPS data. Using relatively low-resolution computational grids (30 arc s, ∼1 km), they found significant resolution loss compared with high-resolution runs given the data available. High-resolution bathymetric and topographic grids are needed to differentiate a variety of source models. The tsunami inundation models used in this study compute the tsunami flooding with telescoping grids of increasing resolution; the finest grid uses a resolution of 2 arc s (∼60 m) to compute the tsunami inundation. This approach also addresses the low-resolution problem raised by MacInnes *et al.* (2013). It is worth noting that the seafloor deformation offshore of the Sanriku Coast of Japan identified by the real-time tsunameter inversion of the NOAA Center for Tsunami Research (NCTR) (Tang *et al.*, 2012; Wei *et al.*, 2013) was further confirmed by MacInnes *et al.* (2013), who concluded that an additional source of tsunamigenic energy is needed to explain high tsunami runup along Japan's east coast between latitude 39°N and 40°N. Similarly, a recent study by Grilli *et al.* (2013a, b) found evidence of a seismically triggered seafloor failure that may be the mechanism responsible for high tsunami runup in the north.

In this study, a total of 11 tsunami inundation models were used to cover the coastline of Japan between latitude 34.5°N and 44.0°N (Fig. 2a). Each of these models contains three telescoped grids with increasing spatial resolution of 2 arc min (∼3.6 km), 15 arc s (∼450 m), and 2 arc s (∼60 m), to compute the tsunami wave dynamics from offshore to onshore.

Tang *et al.* (2009) studied 14 historical events and showed through model validation that a 7–8× variation in grid size provides optimized accuracy and speed for a tsunami forecast model. The bathymetric and topographic grids used in these models were obtained from a combination of the 1-arc-min global relief model of earth surface (ETOPO1), Japan Oceanographic Data Center JODC-expert Grid data for Geography—500 m (J-EGG500), and the GeoSpatial Information Authority of Japan (GSI) 50-m digital elevation model. The GSI digital elevation models also contain 5-m Light Detection and Ranging (LIDAR) data for several small areas. These datasets have different limitations in data quality and data density that may degrade the model accuracy. Wei *et al.* (2013) showed that the large error in the USGS Shuttle Radar Topography Mission 3-s topography resulted in significant underestimation of the inundation limit in the Sendai Plain.

Tsunami impact in the near field, compared with the far field, is more dependent on source geometry (Okal and Synolakis, 2004). This comparative study allows us to examine how source models inferred from different methods fit the measured tsunami impact along Japan's coastline. It focuses on how to utilize these methods to achieve rapid and accurate tsunami hazard assessments in the near field, provided these measurements are available in real time for future earthquakes.

Lastly, this study provides discussion on the utilization of rapidly available measurements that may lead to improved real-time tsunami model forecasts, addressing: (1) What are the characteristics of the source? (2) What are the strengths and limitations of these methods? and (3) How could these methods be utilized to expedite tsunami warning, especially in the near field?

3. Source Models of the 11 March 2011 Japan Tsunami

3.1. Tsunami Source Derived from Tsunameter Measurements

Located 500 km east of the epicenter, tsunameter D21418 measured a 1.8-m-high pulse within 30 min of the earthquake (Fig. 1a). This is the largest tsunami
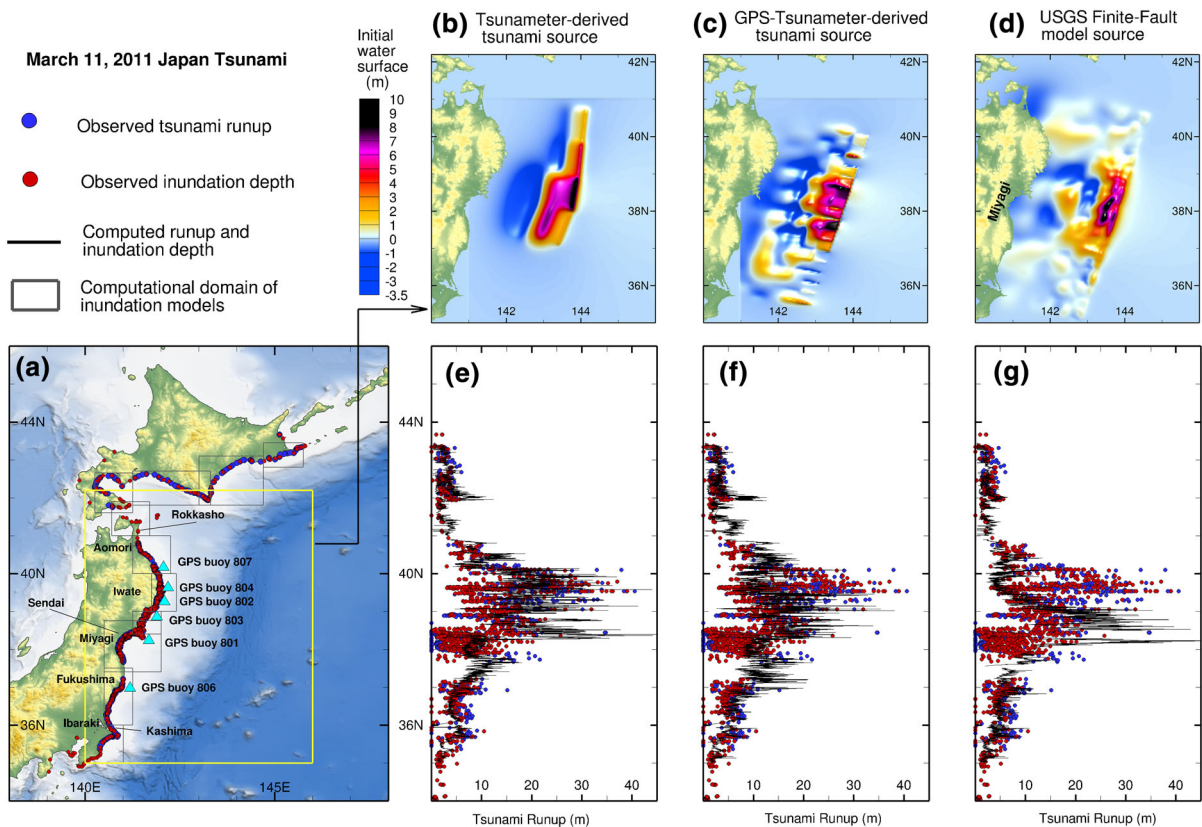
Figure 2
Model–observation comparison of 11 March 2011 Japan tsunami runup height. **a** Model setup along Japan's Pacific coastline, where the *yellow box* corresponds to the domain boundary of the tsunami source computation, and the *cyan triangles* indicate the locations of the Japan Nationwide Ocean Wave information network for Ports and Harbors GPS buoys. *Upper panel* **b** tsunami source derived from tsunameter measurements; **c** tsunami source derived from GPS and tsunami measurements; **d** tsunami source obtained based on USGS finite-fault solution. *Lower panel* **e** comparison between computed and observed tsunami runup for the tsunameter-derived source; **f** comparison between computed and observed tsunami runup for the tsunameter/GPS-derived source; **g** comparison between computed and observed tsunami runup for the USGS finite-fault solution

wave ever recorded by a deep-ocean tsunameter (Tang et al., 2012). The tsunami forecast system of NCTR used records at tsunameters D21418 and D21419 to estimate the tsunami source in a rapid inversion process developed by Percival et al. (2010). Rapid forecasts based on this method rely on developing an a priori database of precomputed tsunamis from a network of subfault patches parameterized to represent global subduction zones (Gica et al., 2008). With rupture dimensions of 100 km × 50 km and 1-m slip, each of these unit sources represents the tsunami source generated by an M_w 7.5 earthquake. MOST computes the tsunami propagation with an ocean basin grid at 4-arc-min resolution for all unit sources. All the

computational results are stored in the tsunami propagation database of NCTR. The precomputed tsunamis are used with real-time tsunami observations from bottom-pressure gages in the deep sea to estimate the approximate tsunami source (Wei et al., 2008; Tang et al., 2009; Titov, 2009). This provides a quick estimate of the seafloor deformation over the tsunami generation area. During the Tohoku event, NCTR first computed a preliminary inversion of the tsunami source 56 min after the earthquake initiation with just station D21418. Upon the passage of the first tsunami peak at station D21401, 990 km northeast of the epicenter, a second inversion was carried out 90 min after the earthquake using the half-wave period

Table 1

Tsunami forecast source constrained from deep-ocean tsunami measurements at tsunameters D21418 and D21401

Unit source	Location	Strike	Dip	Rake	Depth (km)	Source coefficient (m)
1	143.5273E, 40.3125N	185	19	90	5.0	4.66
2	143.4246E, 39.4176N	185	19	90	5.0	12.23
3	143.2930E, 38.5254N	188	19	90	5.0	21.27
4	142.7622E, 38.5837N	188	21	90	21.3	26.31
5	143.0357E, 37.6534N	198	19	90	5.0	4.98
6	142.5320E, 37.7830N	198	21	90	21.3	22.75

Each unit source has dimensions of 100 km length and 50 km width. GICA *et al.* (2008) provide details of the acronyms for all unit sources. The numbering of the unit sources corresponds to that shown in Fig. 1a. The location of each unit source represents the center of the deformation rectangle side parallel to the foot wall (on the subsidence side of the rectangle)

measured from both stations D21418 and D21401. This provided a refined estimate of the tsunami source (Table 1) and indicated that the initially disturbed water surface was from a source with as much as 10 m of sea surface uplift (Fig. 2). Additionally, this model showed that the seafloor deformation was best described by a source rupture 400 km along strike and 100 km landward from the Japan Trench. Based on this tsunameter-derived source, real-time model inundation forecasts for 30 coastal communities in US territories were accomplished within 30 min of obtaining the tsunami source (i.e., 2 h after the earthquake), nearly 5 h before the tsunami struck the Hawaiian Islands, and 7 h before hitting the West Coast of the continental USA (TANG *et al.*, 2012). The same source was used for real-time model prediction of the tsunami heights in New Zealand (BORRERO *et al.*, 2013). The local civil defense increased the hazard level there after model-predicted wave heights were shown to be larger for the tsunameter inverted source than for a uniform slip case. We emphasize that the data (from two tsunameters) used to determine this tsunami source are only a small subset of tsunami records that we use in this study. TANG *et al.* (2012) provided validation of this tsunami source using measurements at 28 additional tsunameters throughout the Pacific. BORRERO *et al.* (2013) reported that their real-time model predictions along the coast of New Zealand were accurate despite the coarse nearshore bathymetry used in the assessment. The tsunami wave measurements and surveyed runup and inundation data in Japan (MORI *et al.*, 2011) provide data to further validate this source in the near field, as discussed in Sect. 4.

3.2. *Combined Tsunameter/GPS Determination of Earthquake Rupture*

Hundreds of GPS stations operated by the GPS Earth Observation Network (GEONET) of Japan recorded the onland deformation caused by the 11 March 2011 Tohoku earthquake. Computation of the raw GPS signals from the Geospatial Information Authority (GSI) of Japan, using preliminary satellite orbit estimates by the Advanced Rapid Imaging and Analysis (ARIA) project at the NASA Jet Propulsion Laboratory and Caltech (OWEN *et al.*, 2011), indicated large-scale ESE seaward displacements as large as 5.2 m horizontally and 1.1 m vertically downward (Fig. 1). These data indicated a very large coseismic rupture offshore and were subsequently corroborated by later available seafloor geodetic observations using the GPS/acoustic combination technique at five sites, which measured between 5 and 24 m of east-southeast horizontal motion and between −0.8 and 3 m of uplift (SATO *et al.*, 2011).

In order to evaluate the earthquake rupture extent and tsunami potential geodetically, we took the unique approach of combining the earliest available ARIA GPS displacement solutions with predictions of the seafloor vertical displacement from the early MOST tsunameter inversions using predefined Green's functions for an existing fault database. The tsunami-predicted vertical seafloor motion as estimated using OKADA (1985) was used instead of the predicted thrust on individual segments because the a priori subduction interface along the Japan Trench did not well represent the current state of knowledge about the slab geometry, and dipped about twice as

steeply as the currently accepted value of 10–12° dip as described in Slab 1.0 (HAYES *et al.*, 2012).

To evenly distribute the data selection between the seafloor uplift estimates (Fig. 2b) and the onland GPS (Fig. 1b), we selected a grid of 77 seafloor estimates along a 0.5° × 0.5° grid along the rupture area and the surrounding region including sections seaward of the trench (142–145°E, 36–41°N). Each of these 77 seafloor vertical estimates was given a factor of 3 weighting over the onland GPS stations to account for the comparable loss in components (1 component offshore, 3 components onland). We used 366 GPS stations nearest the rupture area (138–142°E, 35–42°N) and assigned error estimates to be 10 cm in each horizontal component and 20 cm in the vertical. The offshore vertical estimates were all assigned 20 cm error. The selection for errors, weighting, and discretization of seafloor vertical estimates is somewhat arbitrary, but corresponds to our normal relative confidence between horizontal and vertical GPS data, as well as our sensitivity to seafloor changes in tsunami excitation. Overall, the effects of errors on model predictions are directly dependent on the choice of weighting that we used. While more precise station-dependent and location-weighted errors could be constructed through substantial postprocessing, such details are not readily available for rapid assessments and hence are not considered here.

The onland GPS data and seafloor vertical displacement predictions were inverted using the geometry shown in Fig. 1b (520-km-long fault striking S15W from 144.4°E, 40°N, and dipping 10° west, including 16 along-strike and 8 down-dip segments from 0 to 50 km depth) and a smoothness trade-off with misfit as described in CHEN *et al.* (2009). The preferred slip solution was found at an inflection point at which decreased roughness (increased smoothing) began to substantially increase misfit. The final solution (Fig. 1b) agrees well with onland GPS and seafloor vertical estimates (RMS = 2.8 cm in horizontal and 3.9 cm in vertical). Likewise, the horizontal projection of the thrust component agrees well with horizontal seafloor displacements later determined by SATO *et al.* (2011). Because the near-field tsunameter inversion results (Fig. 2b) were inputs to this inversion, and the final results were

perturbed by onland GPS data and model smoothing, the newly predicted tsunami runup and open-ocean tsunami waves were somewhat degraded (peaks not as well fit). However, the results still match well, and are in almost complete agreement with the onland GPS data.

One interesting feature of this GPS/tsunameter solution is that it shows the utility of the method regardless of whether the predefined faults for the original tsunami inversion were accurate (i.e., whether their assumed geometry reflects the true geometry of the source fault). However, one could argue that, for such solutions in the future, predefined MOST tsunami solutions need not go back to a priori fault characterizations, but instead should just describe discrete pistons of vertical motion, which can be used directly with available onland GPS data to obtain the full cross-shore geodetic solution.

3.3. Finite-Fault Source Derived from Seismological Data

The rapid finite-fault source model for the Japan earthquake was constrained from Global Seismographic Network broadband waveforms based on an inversion algorithm developed by JI *et al.* (2002), and is discussed in greater detail in HAYES (2011) and HAYES *et al.* (2011). This approach inverts teleseismic body- and surface-wave data for the slip amplitude, direction, rise time, and rupture initiation time of a collection of subfaults that make up the fault surface. The fault planes used in the inversion were defined using the US Geological Survey (USGS) National Earthquake Information Center (NEIC) W-phase moment tensor solution, adjusted to match local slab geometry (HAYES *et al.*, 2012). The initial fault size used in the inversion procedure is established using empirical relations between magnitude and fault length and width (e.g., BLASER *et al.*, 2010). Subfault source time functions are modeled with an asymmetric cosine function (JI *et al.* 2002, 2003), and the velocity model used for Green's function computation is based on a combination of Preliminary Reference Earth Model (DZIEWONSKI and ANDERSON, 1981) and Crust 2.0 (BASSIN *et al.*, 2000).

The preliminary solution, made publicly available several hours after the earthquake, predicted a

maximum 17.5 m of slip on a nodal plane striking 195° and dipping 14°, and a corresponding seismic moment of 4.0×10^{29} dyne cm (M_w 9.0) (http://earthquake.usgs.gov/). An updated solution resolved nearly twice the amount of maximum slip—33 m—on a nodal plane striking in the same direction but slightly more shallowly at 10° (Fig. 1c). The seismic moment of the updated solution is 4.9×10^{29} dyne cm (M_w 9.1), an approximately 20 % increase over the preliminary solution. For tsunami modeling, the source parameters of the finite-fault solution are used as input in MOST to compute the ocean surface deformation for each subfault, which first describes the seafloor vertical motion using OKADA (1985). They are then linearly combined to obtain the initial disturbance to the ocean surface (i.e., the tsunami source of the finite-fault solution).

3.4. Characteristics of the Initial Source Deformation

The three source deformations illustrated in Fig. 2, although derived from different methods, share some important features: all source models estimate up to 10 m of vertical displacement near the trench; all models infer the largest displacement to have occurred in the segment between latitude 37.5°N and 39°N; and all models indicate a similar east–west rupture width of about 100 km.

One of the main differences among the source models in Fig. 2a–c lies in the along-strike slip distribution. NOAA's tsunameter-derived source (Fig. 2a) suggests that the water surface along the trench between latitude 39°N and 41°N, at the northern end of the rupture, was uplifted by up to 6 m. This northern extent of the water surface disturbance was not evident in source models derived from seismic and/or GPS data alone. WEI et al. (2013) indicate that this northern disturbance was responsible for the high tsunami along Sanriku's coastline. After examination of nine source models, MACINNES et al. (2013) confirmed that such an additional source of tsunamigenic energy is needed to explain the high tsunami runup along Japan's east coast between latitude 39°N and 40°N. GUSMAN et al. (2012) inferred that this additional uplift originated from motion of a sedimentary wedge that also caused

the large tsunami associated with the 1896 Sanriku earthquake. A recent study by GRILLI et al. (2013a) investigated a possible seismically triggered seafloor failure in the same region, which could also explain this water surface disturbance. One can also see that the tsunameter-derived source estimates an initial subsidence of up to 3.5 m, which decreases westward to less than 0.5 m when reaching the coastline of Honshu (Fig. 2a). The GPS/tsunameter source shows similar results for the largest subsidence, with scattered uplift over the shelf and coastline. The finite-fault source, however, indicates a main subsidence between 38°N and 39.5°N, and a secondary uplifting crustal movement over the shelf offshore of Miyagi (i.e., fault slip and thus seafloor uplift extending farther downdip).

Another difference among the source models is that both the GPS/tsunameter source model and the finite-fault model show 10–15 m of slip along the updip portion of the southern rupture area, where the tsunameter-derived source model indicates no disturbance. This is probably due to the size of the unit sources in the tsunameter model (100 km × 50 km), which usually filters out negligible water surface disturbances when they are linearly combined for an inversion process. The small subfaults employed in the GPS/tsunameter and finite-fault methods are useful for resolving detailed slip distributions of earthquake rupture. We note though that the increase in degrees of freedom resulting from small subfaults adds more uncertainty to the inversion solution, and thus may delay the dissemination of a valid tsunami warning and forecast. HAYES (2011) discussed that additional constraints, such as a priori fault geometry, and bounds to rupture velocity and peak slip, can speed up finite-fault inversions.

It is worth noting that, in the three source models that we compare in this study, the number and azimuthal distribution of observing stations are very different. The tsunameters are sparsely, but optimally, placed in the Pacific Ocean. During an event, the tsunameter inversion process starts after the earliest observation (most likely at the closest station to the source), such as 21418 in Fig. 1. However, measurements from a second tsunameter located off the main focus of tsunami energy, such as 21401, will improve the inversion results. Ideally, three

tsunameters encompassing the main focus of the tsunami energy (such as 21418, 21401, and 21413) provide a robust estimate of the tsunami source. TANG et al. (2012) compared the inversion results of the tsunami source (used in this study) based on one (21418), two (21418 and 201401), and three tsunameters (21418, 21401, and 21413). They showed that the inversion using two tsunameters improved the tsunami energy estimate by 20 % from the inversion using only one tsunameter, while little more information was gained (6 %) from the inversion using three tsunameters. For the joint GPS/tsunameter solutions, resolution in the portion that most affects tsunamis is poorly constrained by GPS alone, given that the nearest stations are approximately 200 km from the updip edge of the slip models, the region most responsible for tsunami generation. In inversions tested using only GPS data we found similar downdip slip values; however, the more distal updip region had a maximum of only 33 m of thrust motion. Determining the true offshore patch-size resolution of this model is difficult because seafloor uplift estimates use predictions reconstructed from tsunami-derived interface slip models. Thus, for these results the farthest offshore points will have resolution patches comparable in size to the surface expression of the tsunami slip patches (100 km along-strike and about 50 km downdip). For the seismic solution, data are selected such that they are evenly distributed azimuthally around the source, and thus provide an optimal configuration for minimizing azimuthal bias on the model solution, though observations are inherently farther from the source because of the teleseismic nature of the inversion. HAYES (2011) discussed resolution tests of the seismic models; we refer readers there for more detail.

4. Model Results

The posttsunami survey by Japanese scientists provided data of tsunami runup (or inundation depth) and inundation limits at nearly 3,000 locations along the Pacific coastline of Honshu and Hokkaido (MORI et al., 2011; Fig. 2). The largest tsunami runup they identified was 39.7 m in the Omoe Aneyoshi District

of Miyako, Iwate Prefecture (MORI et al., 2011). The latitudinal distribution of tsunami runup and inundation depth shows that high runup ($\geq$20 m) was mostly focused along the coastline between 39°N and 40°N, where many narrow valleys are found that may have funneled the tsunami waves to much higher elevations. Runup height along the coastline changes abruptly from greater than 30 m to less than 10 m, at 40.2°N in the north and 36.8°N in the south, which approximately corresponds to the northern and southern extent of the high-uplift zone.

4.1. Tsunami Runup Height and Inundation Depth along Japan's East Coast

WEI et al. (2013) and MACINNES et al. (2013) both pointed out the importance of using high-resolution model grids to reproduce the high runup between 39°N and 40°N. MACINNES et al. (2013) showed that a grid resolution of 30 arc s ($\sim$900 to 1,000 m) was not enough to resolve the detailed coastal features, and led to an underestimation (by 10 to 20 m) of the runup height and inundation depth north of 39°N. Therefore, we have applied the same tsunami inundation models as in WEI et al. (2013) with grid resolution of 2 arc s ($\sim$60 m) for all three source models. All models reproduce the smaller runup well, but show differences in matching the high runup values, especially between 39°N and 40°N (Fig. 2e–g). The runup computed from the tsunameter-derived source model fits well with the measurements for both high and low runup, and also reproduces the sharp changes in runup height at the ends of the rupture well (Fig. 2a). The tsunameter-derived source (Fig. 2e) can also successfully reproduce the highest runup of 39.7 m at Omoe Aneyoshi (39.5337°N, 142.046°E), though the model slightly underestimates the runup heights and inundation depths along the coastline of Sendai (between 38°N and 38.3°N). Compared with the tsunameter-derived source model, the GPS/tsunameter-derived model reproduces observations better in the low-runup segments, but underestimates runup heights by almost 10 m in the high-runup area between 39.5°N and 40°N (Fig. 2f). This model also matches the tsunami measurements in the Sendai Plain well. The updated USGS finite-fault source model also reproduces low runup well,

but significantly underestimates the high-runup zone between 39°N and 40°N (Fig. 2f). This indicates an inadequate tsunami source representation in the northern portion of the model. Despite issues in matching the highest runup in the north, the overall distributions of the modeled runup heights along the coastline from all three models are encouraging, especially for the two source models that used the tsunameter measurements (Fig. 2a, b).

4.2. Deep-Ocean Propagation

The time series recorded by the tsunameters are used not only for quick constraint of the tsunami source, but also for providing validation of the model forecast for distant coastlines in real time. The model–data comparisons provided in Fig. 3 show that all source models were able to achieve excellent matches to tsunami arrival times at stations D21418 and D21413. The leading peak wave computed from the GPS/ tsunameter source and the finite-fault solution are slightly out of phase with the observations at stations D21401 and D21419. The GPS/tsunameter source suggests an arrival time approximately 3 min earlier than observed, and the finite-fault solution implies an arrival 5 min earlier than observed. These phase mismatches indicate a range of 10 to 20 km error (less than 5 % error with respect to a 400-km rupture length) in prediction of the high-slip-patch location from different source models. The excellent agreement with the time series at all four tsunameters shows the credibility of the tsunameter-derived source (Fig. 3a), beyond the two stations used to produce the model. Table 2 indicates that the tsunameter-derived source produces a model accuracy of 91.6 % in predicting the maximum tsunami wave amplitude at the four deep-ocean tsunameters. The GPS/tsunameter source model also shows very good agreement between the model and measured time series, with the exception of a 41 % underestimate of the first peak recorded at station D21418 (Fig. 3b). This source has a model accuracy of 76.8 % in predicting the maximum tsunami wave amplitude at the tsunameters (Table 2). When comparing the computed maximum tsunami wave amplitudes in the northwestern Pacific Ocean, it is clear that station D21418 is at a location that receives higher tsunami energy from the tsunameter-derived

source model (Fig. 3a) than from the GPS/tsunameter-derived source model (Fig. 3b). Again, we attribute this difference to the higher uplift in the northern portion of the rupture in the tsunameter-derived source model than was present in the other two. The seismic source model (which did not include any tsunami data in its inversion) also provides excellent estimations of the first peak at all four tsunameters, as indicated by the model accuracy of 91.6 % for the maximum tsunami wave amplitude (Table 2). This source model implies a second positive pulse that does not match the observed depression after the first peak, which is likely caused by the secondary uplift to the east of the main rupture area (Fig. 3c). The corresponding maximum wave amplitude map indicates that this source model produces the least tsunami energy among the three, whereas the tsunameter-derived source produces the most.

To better quantify the model results, we compared the wave spectrum of the modeled time series against the observations at all tsunameters. Figure 4 shows that all source models give reasonable prediction of the observations in the frequency domain. At tsunameters D21401, D21419, and D21413, all source models produce results concordant with the observations for wave periods up to 40 min. Wave periods greater than an hour registered at these deep-ocean tsunameters may belong to the background noise rather than the tsunami signatures themselves (ZHOU et al., 2014). It is worth noting that all modeling results provide good agreement at high frequencies (wave period between 1 and 10 min), suggesting that the modeling results also predict the trailing waves well. Modeling results from the tsunameter-derived source show the best agreement with the spectral energy at wave periods between 10 and 40 min, whereas the other two sources slightly underestimate for wave periods of 20 min and greater. At station D21418, the tsunameter-derived source presents better agreement for wave periods less than 10 min relative to the other two source models.

One would expect good agreement between the computed and observed time series at tsunameters D21418 and D21401, as they were used to directly obtain the tsunami source. Merely retrieving the various time series used in the joint inversion is certainly not proof of better forecasting ability of the tsunameter method. We therefore compared the computed results at other tsunameters (e.g., 21413
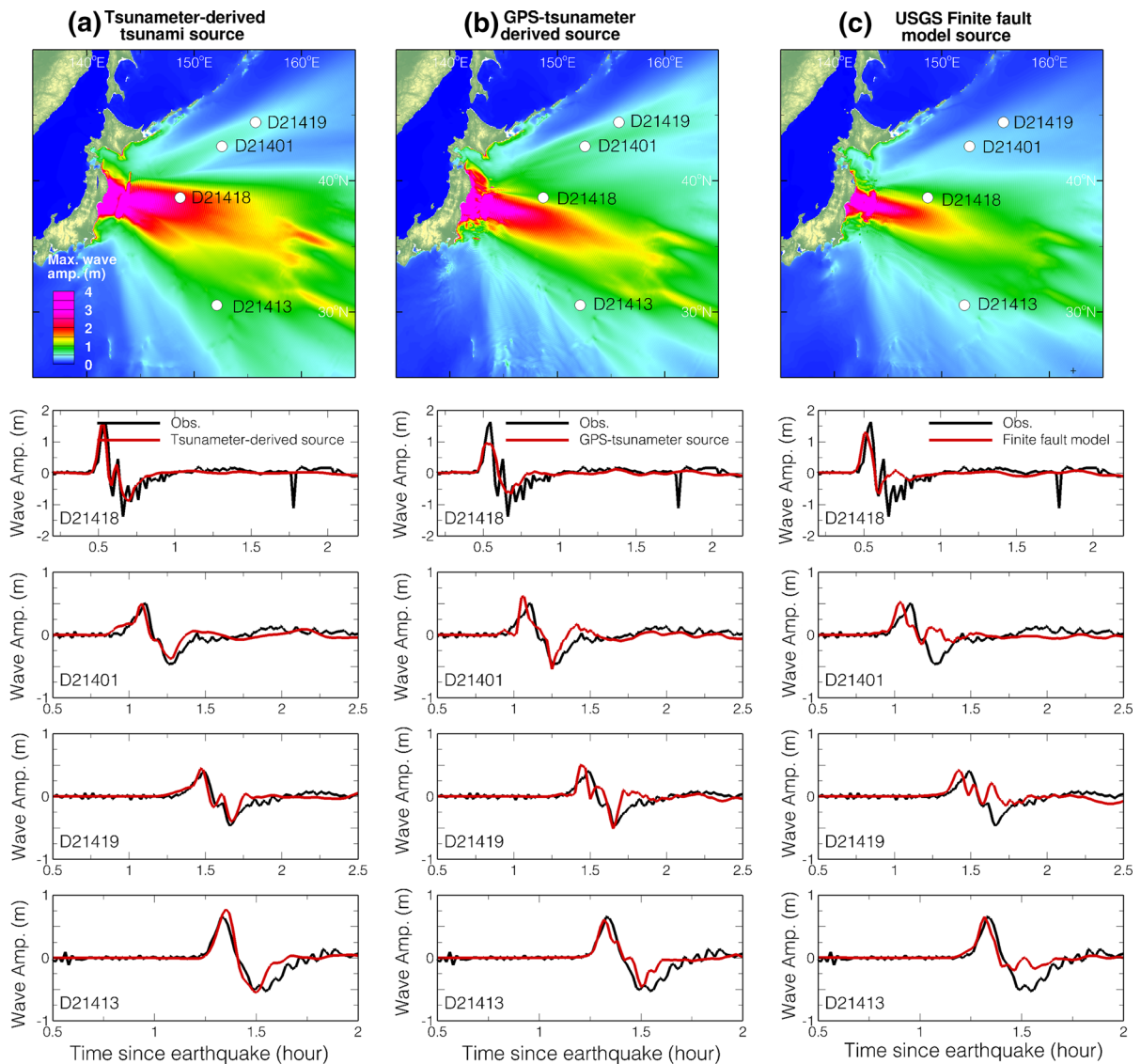
Figure 3

Model–observation comparison of 11 March 2011 Japan tsunami waveforms at deep-ocean tsunameters. **a** *Upper panel* maximum tsunami amplitude obtained using the tsunameter-derived source; *lower panel* comparison between computed and observed tsunami waveforms, where model results are obtained using the tsunameter-derived source. **b** *Upper panel* maximum tsunami amplitude obtained using the GPS/tsunameter-derived source; *lower panel* comparison between computed and observed tsunami waveforms, where model results are obtained using the GPS/tsunameter-derived source. **c** *Upper panel* maximum tsunami amplitude obtained using the finite-fault model source; *lower panel* comparison between computed and observed tsunami waveforms, where model results are obtained using the finite-fault model source

and 21419 in Fig. 3) to verify the source derivation based on tsunameters D21418 and D21401. TANG *et al.* (2012) presented comparisons at 30 tsunameters throughout the Pacific Ocean. In this study, we provide further evidence of the successful performance of this method using model-independent results such as nearshore measurements (Sect. 4.3), runup (Sect. 4.1), and inundation (Sect. 4.4).

4.3. *Nearshore Transformation of the Tsunami Waves*

The GPS buoys deployed by the Japan Nationwide Ocean Wave information network for Ports and Harbors (NOWPHAS) (KATO *et al.*, 2000, 2008) provided real-time measurements of tsunami propagation over the continental shelf between the Japan

Table 2

Comparison of maximum tsunami wave amplitude between models and observations at deep-ocean tsunameters and nearshore Japan Nationwide Ocean Wave information network for Ports and Harbors GPS buoys

	Station	Observed max. tsunami amp., A_{obs} (m)	Modeled max. tsunami amp. (m) and E (%)		
			Tsunameter-derived source	GPS/tsunameter source	Seismic source
Deep ocean	D21418	1.63	1.57 (−3.7 %)	0.96 (−41.1 %)	1.28 (−21.0 %)
	D21401	0.50	0.50 (0 %)	0.61 (+22.0 %)	0.53 (+6.0 %)
	D21419	0.40	0.44 (+10.0 %)	0.50 (+25.0 %)	0.42 (+5.0 %)
	D21413	0.65	0.78 (+20.0 %)	0.62 (−4.6 %)	0.66 (+1.5 %)
Model accuracy			91.6 %	76.8 %	91.6 %
Nearshore	GPS807	4.02	3.50 (−12.9 %)	2.92 (−27.4 %)	1.18 (−70.6 %)
	GPS804	6.30	5.42 (−14.0 %)	2.52 (−60.0 %)	1.68 (−73.3 %)
	GPS802	6.17	5.64 (−8.6 %)	3.07 (−50.2 %)	2.80 (−54.6 %)
	GPS803	5.18	5.28 (+1.9 %)	3.75 (−27.6 %)	7.80 (+50.6 %)
	GPS801	4.78	7.55 (+57.9 %)	6.17 (29.1 %)	7.80 (+63.2 %)
	GPS806	2.12	1.33 (−37.3 %)	2.71 (27.8 %)	1.82 (−14.2 %)
Model accuracy			77.9 %	63.0 %	45.6 %

The error E is calculated as $E = (\eta_m - \eta_{obs})/\eta_{obs} \times 100$ %, where η_{obs} is the observed maximum tsunami amplitude at the station and η_m is the computed maximum tsunami amplitude. The model accuracy is calculated as $1 - (\sum |E|)/n$, where n is the number of stations used for error calculation

Trench and the Honshu coastline. If one considers the tsunameter comparison as a validation of the tsunami propagation on the uplifted side of the source, then the NOWPHAS buoy (Fig. 2) measurements allow us to look closely at the tsunami wave dynamics on the subsided side of the tsunami source. Since all NOWPHAS buoys are deployed at water depths between 100 and 250 m, their measurements are not affected by the rugged coastline (which becomes particularly complex in Iwate). These buoy measurements contain direct information about the origin of the tsunami. The spatial coverage of these buoys from Iwate in the north to Miyagi in the south also offers a good calibration of the slip distribution along the length of the rupture. In Fig. 5, one can see that the pattern of GPS buoy observations from north to south is consistent with that shown by the runup height and inundation depth along the coast: large offshore waves (up to 6.3 m) corresponding to high tsunami runup were recorded between latitude 38°N and 40°N, and decayed further north and south. All three source models produce good estimates of the offshore waveforms, including the trailing waves, at the three NOWPHAS GPS buoys in the south (GPS buoys 803, 801, and 806) in terms of wave amplitude and period. The largest difference among the source model

predictions is seen for GPS buoys 804 and 802 located offshore of Iwate. The tsunameter-derived source model produces excellent agreement of the time series at these two buoys, especially the 6-m-high amplitude registered for the first wave. This source produces modeling results with small errors, about 14 % at GPS804 and 8.6 % at GPS buoy 802, in comparison with the observations. The GPS/tsunameter-derived source model gives a 50 % lower estimate for the first wave at GPS buoy 802, and a 60 % lower estimate for the first wave at GPS buoy 804. The seismic source model underestimates by about 73.3 and 54.6 % the first wave amplitude at GPS buoys 804 and 802, respectively, indicating that its tsunami source estimate in the north was not sufficient where a nonseismic seafloor failure might be the dominant tsunami generation mechanism (GRILLI et al., 2013b). Table 2 shows that the average model accuracies (in terms of maximum tsunami wave amplitude) at all six GPS buoys are 77.9, 63.0, and 45.6 %, respectively, for the tsunameter-derived, GPS/tsunameter-derived, and seismic sources, respectively. Again, the initial water surface deformations in Fig. 2b–d clearly show the differences between the three source model predictions between 39°N and 40°N: (1) The tsunameter-derived
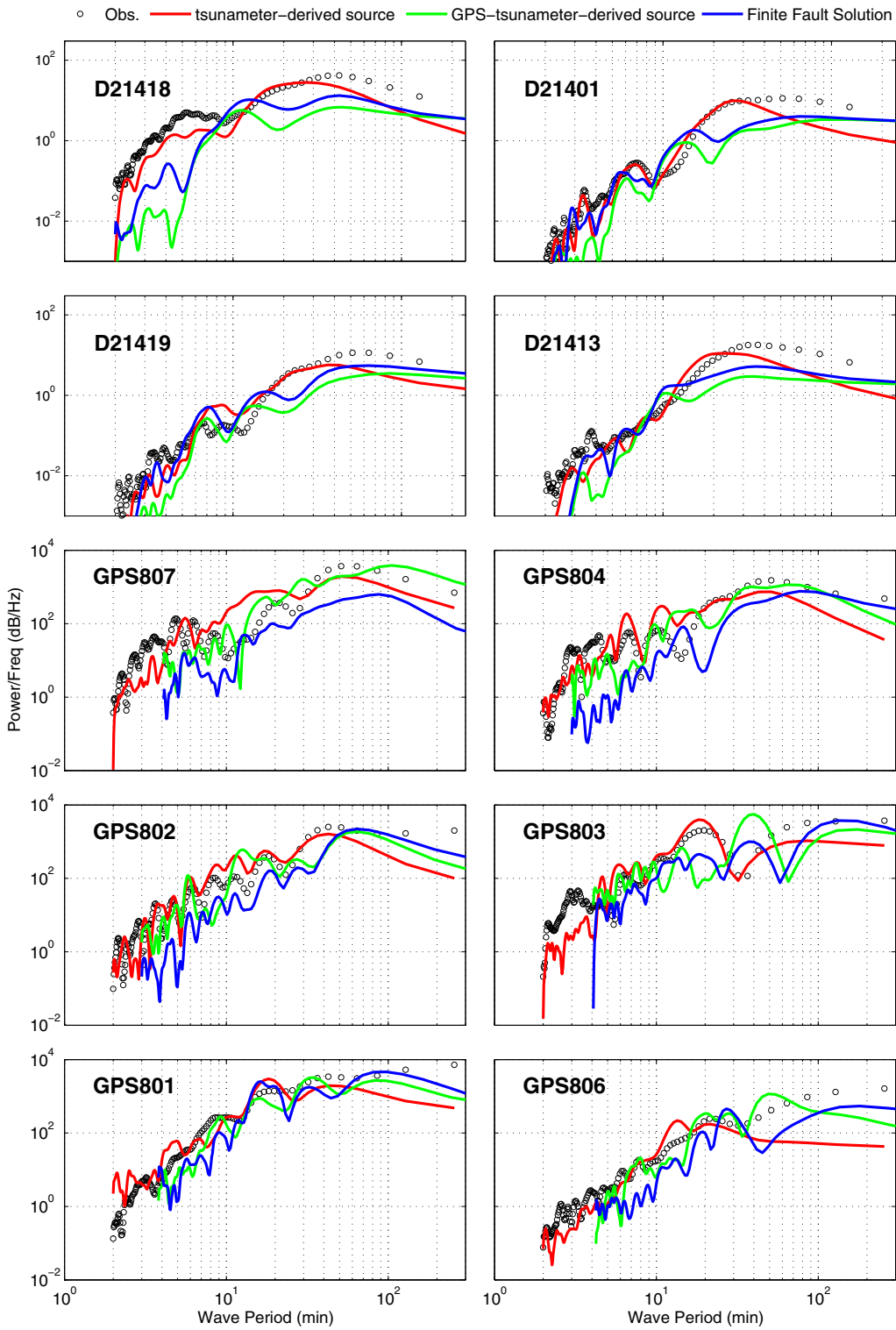
Figure 4
Spectral analysis of modeling results against observations at open-ocean tsunameters and nearshore GPS buoys

source indicates up to 5 m of initial surface deformation, whereas the other two source models predicted less than 1 m. (2) Similar to the tsunameter-derived source, the GPS/tsunameter-derived source predicts the greatest surface deformation—about 10 m (black color in Fig. 2b–d)—between 38.5°N and 39°N, whereas the seismic model's largest surface deformation is concentrated further south near 38°N. The GPS/tsunameter-derived source produces better predictions of the tsunami height at GPS buoys 807 and 802 compared with the seismic model. The underestimation by both of these models at GPS buoy 804 can probably be attributed to the underprediction of the surface deformation between 39°N and 40°N (Fig. 2c). Despite their different estimates of the amplitude of the first wave, all source models provide very good predictions of the trailing waves at all GPS buoys. The spectral analysis in Fig. 4 also shows that the high-frequency components (wave periods between 1 and 10 min) in the trailing waves are captured by the modeling results at all GPS buoys. This phenomenon probably indicates that these trailing waves were more dominated by wave interaction—such as wave shoaling, reflection, and refraction—with the local bathymetry and coastal features, rather than by initial source deformation. WEI et al. (2013) specifically pointed out that these complex wave interactions may not be accurately resolved by a simple semiempirical formulation or coarse grid resolution, and thus a high-resolution nonlinear tsunami inundation model is needed for accurate modeling forecasts. All source models produce very encouraging results for spectral energy, matching the observations (Fig. 4). The tsunameter-derived source and GPS/tsunameter-derived source give more similar results in terms of spectral energy than the seismic source. Although the seismic source slightly underestimates the spectral energy at GPS buoys 807 and 804, it provides good prediction at the other four GPS buoys. The tsunameter-derived source provides good estimation of the waves with period up to 40 min at all GPS buoys. However, it slightly underestimates the energy at wave periods greater than 1 h, especially at GPS buoy 806.

We note here that these forecast models can finish up to an 8-h simulation of tsunami inundation within 20 min, and this can also be significantly shortened to less than a couple of minutes with new computing technology, such as graphics processing unit (GPU) computing or parallel computing on a high-performance computer.

4.4. Tsunami Inundation Along Japan's East Coast

The tsunami inundation surveyed by Japanese scientists (MORI et al., 2011) provides additional validation for the reference source models. The most severe tsunami flooding occurred along the coastline between Sendai and Soma, and farther south to the Fukushima Daiich Nuclear Power Plant (NPP). Here we use the inundation model covering this section of Japan's coastline to illustrate differences among the three source models in predicting the tsunami flooding. As shown in Fig. 6, the inundation computations from all three source models provide very good estimation of the inundation extent along the coast between Soma and the Fukushima Daiich NPP. The GPS/tsunameter combined source model presents the largest inundation extent overall (Fig. 6b), especially in the southern part of Sendai (between latitudes 37.9°N and 38.1°N), where the tsunameter-derived source model slightly underestimates the inundated areas. The inundation distance computed using the seismic source model is the smallest among the three source models. The predictions of the maximum tsunami amplitude offshore from each model clearly correlate with the different estimates of tsunami inundation. In Fig. 2c, the GPS/tsunameter-derived source model produces the smallest uplift along the trench offshore of the Sendai Plain, but higher uplift offshore of the Soma area. This subtle difference leads to distinctly different offshore tsunami amplitude predictions along the Sendai Plain and Soma areas: smaller wave amplitude offshore of Sendai Plain, but larger wave amplitude offshore of Soma. It is worth noting that the GPS/tsunameter-derived source model produces better agreement with the observations from NOWPHAS buoy GPS801 (Fig. 5), implying that this source model may provide better estimates of the initial source deformation for the rupture segment offshore of the Sendai Plain.

To illustrate how the source models vary in predictions of the tsunami impact farther north along Japan's coast, Fig. 7 shows the computed inundations
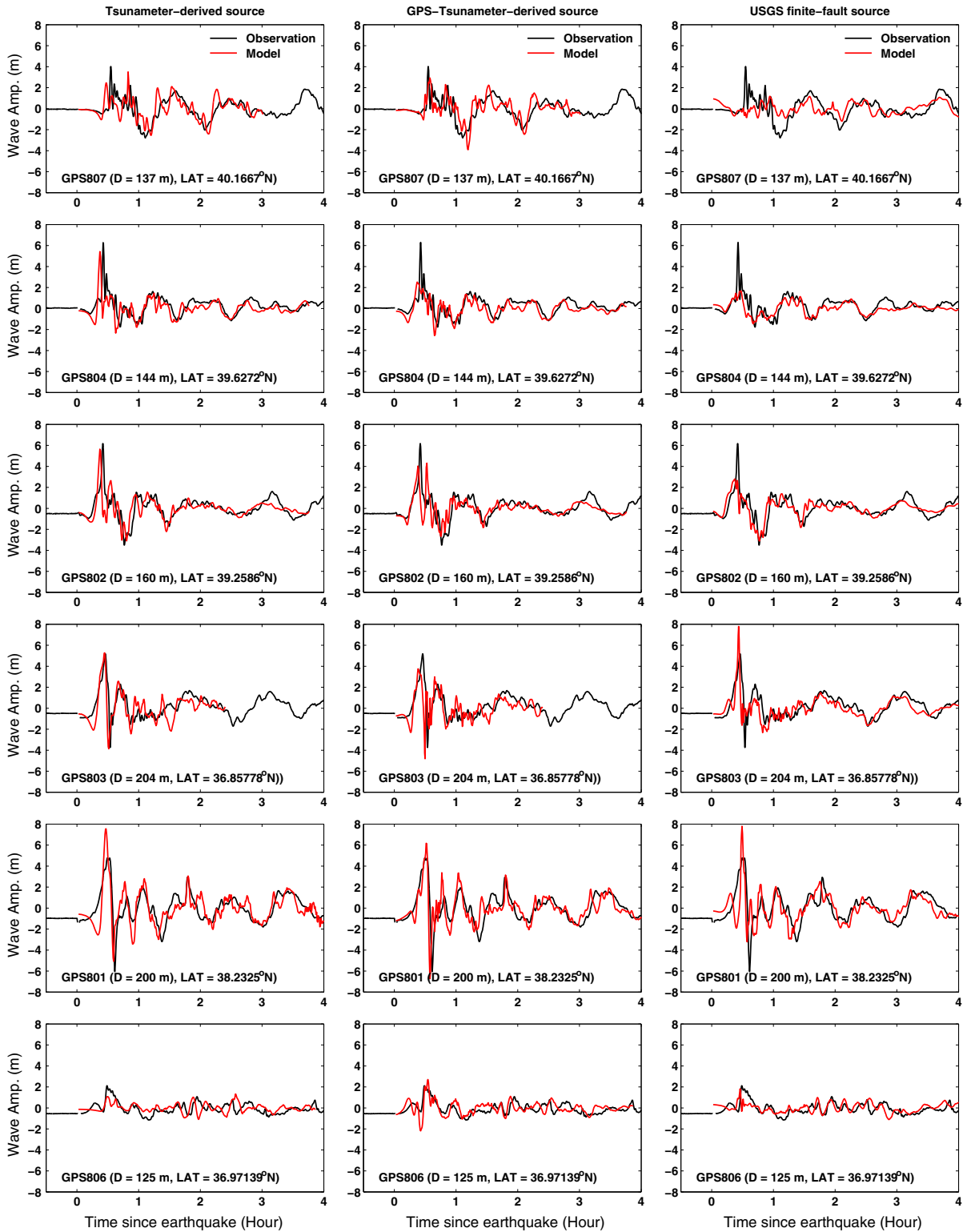
◄

Figure 5

Model–observation comparison of the 11 March 2011 Japan tsunami at NOWPHAS GPS buoys in order from north to south (Fig. 2). *Left panel* comparison between computed and observed tsunami inundation, where model results are obtained using the tsunameter-derived source. *Central panel* comparison between computed and observed tsunami inundation, where model results are obtained using the GPS/tsunameter-derived source. *Right panel* comparison between computed and observed tsunami inundation, where model results are obtained using the finite-fault model source

at three locations from north in Kuji and Noda (Fig. 7a–c) to south in Miyako (Fig. 7d–f) and in Ofunato and Rikuzentakata (Fig. 7g–i). At Rikuzentakata and Ofunato (Fig. 7g–i), all source models predict similar inundation extent. The maximum tsunami water level predicted by the tsunameter-derived source model is about 22 m at Rikuzentakata, whereas the GPS/tsunameter-derived source model and the seismic source model both predict maximum water levels of approximately 15 m

in the same area. These differences lead to contrasting predictions of the inundation extent in the Kesen River Valley. The tsunameter-derived source model provides the best match with the surveyed inundation limit, particularly in the valley west of Kesen River. Farther north at Miyako (Fig. 7d–f), it is clear that the seismic source model significantly underestimates the inundation extent, with only a 2.6 m maximum wave amplitude in the open ocean and up to 4 m in the bay area of Miyako. The tsunameter-derived source model predicts the highest maximum water level along Miyako's coastline of 30 m near cliffs to the east of Miyako, and 26 m along the coastline north of Miyako. Predictions from both the tsunami-derived and GPS/tsunameter source models show good agreement with the observed inundation line. Similar results are seen in the Kuji and Noda areas (Fig. 7a–c), where the seismic source model predicts the lowest estimates of both offshore and onshore water levels, and underestimates the inundation extent at
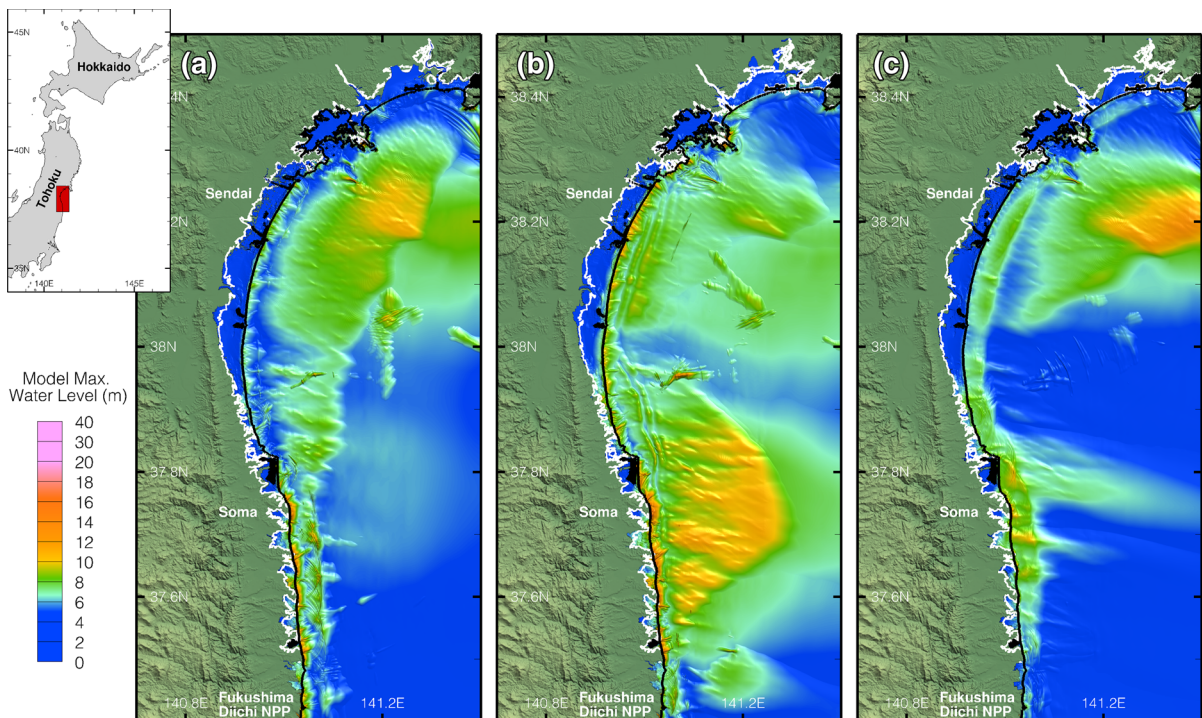

Figure 6

Model–observation comparison of 11 March 2011 Japan tsunami inundation in the areas of Sendai, Soma, and Fukushima, where the *thick white line* indicates the observed inundation limit, and the *color* represents the computed maximum water level. **a** Comparison between computed and observed tsunami inundation, where model results are obtained using the tsunameter-derived source. **b** Comparison between computed and observed tsunami inundation, where model results are obtained using the GPS/tsunameter-derived source. **c** Comparison between computed and observed tsunami inundation, where model results are obtained using the finite-fault model source
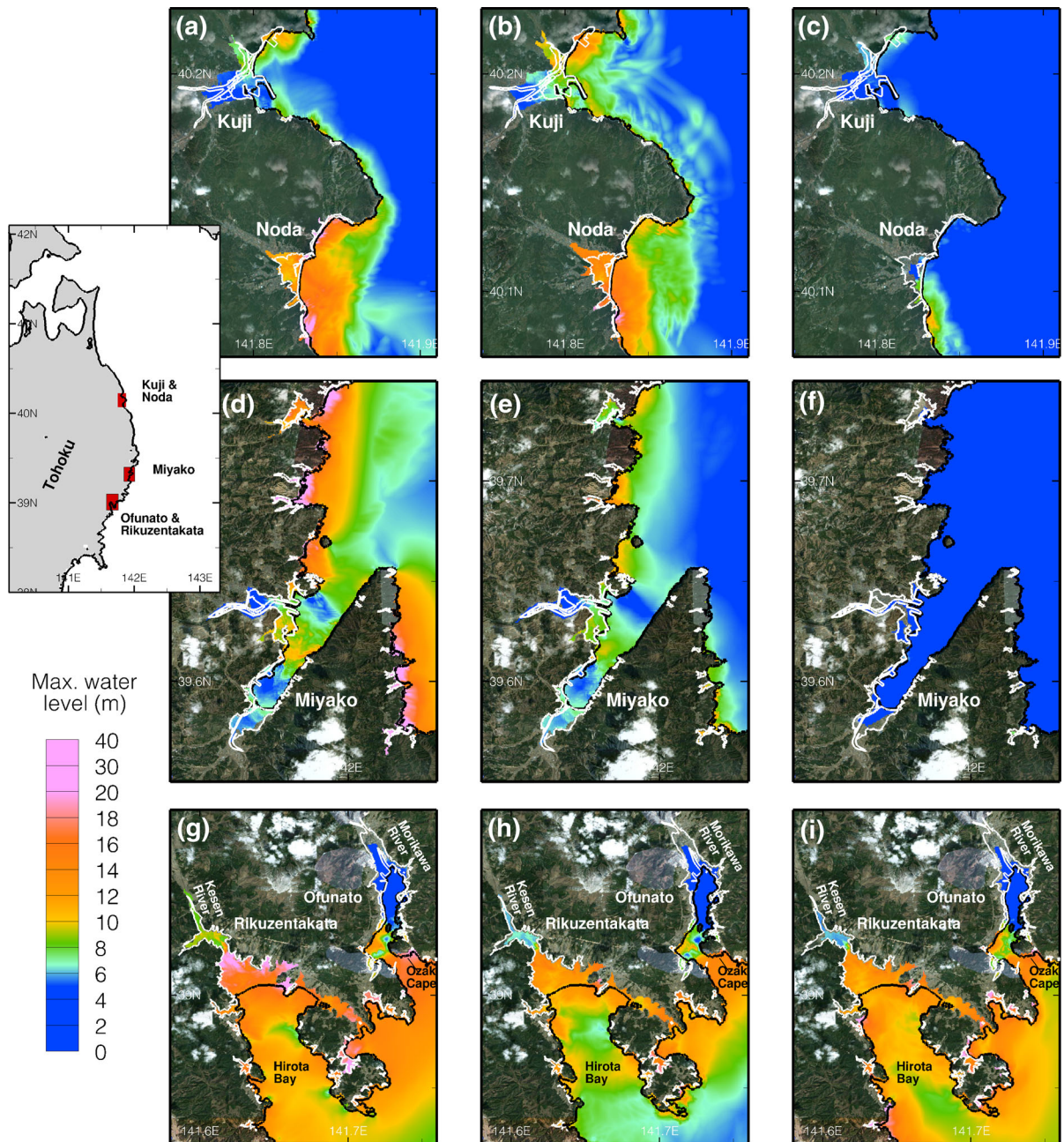
Figure 7

Model–observation comparison of 11 March 2011 Japan tsunami inundation along the coastline in the north of Tohoku Island, where the *thick white line* indicates the observed inundation limit, and the *color* represents the computed maximum water level. **a** Comparison between computed and observed tsunami inundation at Kuji and Noda for the tsunameter-derived source; **b** comparison between computed and observed tsunami inundation at Kuji and Noda for the GPS/tsunameter-derived source; **c** comparison between computed and observed tsunami inundation at Kuji and Noda for the USGS finite-fault solution; **d** comparison between computed and observed tsunami inundation at Miyako for the tsunameter-derived source; **e** comparison between computed and observed tsunami inundation at Miyako for the GPS/tsunameter-derived source; **f** comparison between computed and observed tsunami inundation at Miyako for the USGS finite-fault solution; **g** comparison between computed and observed tsunami inundation at Ofunato and Rikuzentakata for the tsunameter-derived source; **h** comparison between computed and observed tsunami inundation at Ofunato and Rikuzentakata for the GPS/tsunameter-derived source; **i** comparison between computed and observed tsunami inundation at Ofunato and Rikuzentakata for the USGS finite-fault solution

Table 3

Comparison of tsunami inundation accuracy measured by inundated area during the 11 March 2011 Japan tsunami

Prefecture	IA_m (km^2)	Tsunameter-derived source IA_t (km^2)	GPS/tsunameter source IA_g (km^2)	Finite-fault source IA_f (km^2)
Aomori (south of Rokkasho)	19	52	67	11
Iwate	58	58	79	71
Miyagi	327	345	372	174
Fukushima	112	131	155	234
Ibaraki (north of Kashima)	17	24	34	45
RMS (km^2)		19.1	37.2	88.7
L2 accuracy (%)		98.5	94.4	68.2

L2 accuracy $= \sum(I_m^2)/\sum(I_o^2) \times 100$ %, where I_m represents the model-computed inundated area for each prefecture, and I_o represents the observed inundated area in each prefecture

IA_m measured inundated area provided by the Geospatial Information Authority of Japan, IA_t computed inundated area based on tsunameter-derived source, IA_g computed inundated area based on GPS/tsunameter-derived source, IA_f computed inundated area based on USGS finite-fault solution, *RMS* root mean square

both locations. The GPS/tsunameter source model shows slightly higher maximum water levels than the tsunameter-derived source model, especially for offshore wave amplitudes near Kuji Harbor. WEI et al. (2013) specifically discussed the model limitation at a 60-m grid resolution due to a lack of high-resolution topography for these shallow regions, and showed that the hilly bathymetry surrounding Noda was probably more dominant than the seawall in forming focused wave energy in the narrow valleys.

We note that the elastic earthquake deformation formula implemented in the MOST model is based on a rectangular fault model with a uniform slip distribution, and may not completely and precisely predict seafloor displacements from more complicated slip models. In addition, the transformation of the coseismic displacement into ambient water body deformation is one of the most understudied problems in tsunami science to date. The seismic source model also requires further transformation, from fault slip to seafloor deformation. These limitations may result in biased estimates of the tsunami source (or of the initial disturbed water surface). However, the theory of KAJIURA (1970), of an instantaneous transfer of the vertical disturbance at the seafloor to the ocean surface, has been widely accepted and coupled with standard shallow-water models of tsunami wave dynamics, and has performed well in numerous other tsunami model simulations (e.g., TITOV and SYNOLAKSI, 1998; WANG and LIU, 2007; YAMAZAKI et al.,

2011; MACINNES et al., 2013). On the other hand, GRILLI et al. (2013a) used a three-dimensional (3D) nonhydrostatic model to generate the initial tsunami source as a function of the space- and time-dependent seafloor deformation. They compared the subsequent model to one generated using the more typical approach of KAJIURA (1970), specifying the maximum seafloor deformation as the initial free-surface deformation, in the tsunami model and found significant differences. Therefore, to avoid the uncertainties involved in converting a seismic source to a tsunami source, especially for the purpose of tsunami forecasts, deriving a tsunami source from direct tsunami wave measurements can significantly improve the efficiency and accuracy of tsunami forecasts by reducing the number of unknowns. It is worth noting that this tsunami source may not fully represent the physical processes (e.g., the earthquake rupture process) that are responsible for its generation.

Another interesting aspect of the inundation modeling arises from comparisons of the predicted total inundated area with survey results, which present an overall picture of how each source model performs. It is necessary to perform such an analysis region by region, to account for variations in the source model characteristics and coastal topographic features along different parts of Japan's coast. Table 3 presents the total computed inundated areas for each prefecture and comparison with observations provided by the Ministry of Land, Infrastructure,

Table 4

Time of earliest measurements made available for source estimation, first source estimation, and refined source estimation for all three models

Source model	Time of earliest measurements made available for source estimation	Time of first source estimation	Time of refined source estimation
Tsunameter-derived source	30 min	0.9 h	1.5 h
USGS finite-fault source	5–15 min	1.75 h	7 h
GPS/tsunameter source	Several hours[a]	Hindcast	

[a] While rapid "precise point position" solutions were used in this model, immediate real-time kinematic solutions would provide similar quality data and could become available before the earliest tsunami data

Transport, and Tourism (MLIT) of Japan (MLIT, 2011a, b). In a slightly different approach to WEI et al., (2013), here we apply an L2-norm to better describe the model accuracy in each prefecture. Table 3 lists L2-norm accuracies of 98.5, 94.4, and 68.2 %, corresponding to root-mean-square errors of 19.1, 37.2, and 88.7 km^2, for the models derived from tsunameter data, GPS and tsunameter data, and seismic data, respectively. One can see that the tsunameter-derived source model and the GPS/tsunameter source model provide close estimates of the inundated area in all prefectures affected. The modeling results from these two source models also match the spatial change of the inundated area well, i.e., a maximum inundated area in Miyagi Prefecture, decreasing to the north and south. However, the inundated areas computed from the seismic source model overestimate the observations in Fukushima Prefecture, and underestimate those in Miyagi and Aomori (south of Rokkasho). These discrepancies, coupled with the above-mentioned results, indicate that the rapid USGS seismic source model could be further improved, and that including deep-ocean tsunami measurements in the inversion may lead to better prediction of the observed tsunami source. A similar approach is described in YAMAZAKI et al. (2011).

5. Discussion

Among the three source models described in this study, both the tsunameter-derived source and the finite-fault seismic model were rapidly created while the 2011 Japan tsunami was ongoing. The GPS/tsunameter source model was developed afterward but using information that in the future could become available as soon as it is collected; tsunameter data are already relayed in real time, while a number of methods are available for obtaining real-time kinematic GPS solutions with cm-level accuracy relative to nearby, undeformed stations. The seismically defined finite-fault source model employed data from globally available seismic stations. As such, the solution is sensitive to heterogeneity in local velocity structure, and may be biased by uncertainties in the earthquake hypocenter; hence, the models may not be optimal for rapid tsunami forecasts when used alone—particularly in cases where nonseismic seafloor deformations (e.g., landslides or slumps) contribute to the tsunami.

Table 4 presents the temporal availability of the preliminary and refined source models relative to the onset of the 2011 Japan earthquake. While real-time kinematic GPS solutions could yield rapid coseismic rupture propagation and surface displacement fields, no such automated system was available at that time, nor was the implementation of codes for rapid GPS-based source inversions. Moving forward, GPS-based solutions should be shown to be robust, and preferably demonstrated in a large earthquake, before being considered as highly useful real-time tsunami warning tools.

Since the 2011 Japan tsunami, observation and modeling technologies have been improving in terms of the rapidity of solutions. Deep-ocean tsunameters can be deployed closer to the source region to detect tsunami signals quickly, in 10–20 min. Some rapid data products were made available with 2-h latency after the September 2012 Nicoya, Costa Rica earthquake (YUE et al., 2013). Networks are being established to provide real-time kinematic GPS data

for Cascadia (Rabak *et al.*, 2010) and Southern California (Langbein and Bock, 2004; Crowell *et al.*, 2012). The problem with GPS networks remains that they are currently limited to onshore, and usually lack the necessary geometry to reproduce the true source with fidelity. Over the coming decade, teleseismic finite-fault models will likely remain the best first information about the rupture details of an earthquake. However, the inclusion of real-time GPS data, when geographically available, is invaluable to help constrain the lateral position and dip of a rupturing fault. Rapid deep-ocean tsunami measurements can help resolve the location, and particularly the near-trench extent, of seismically derived finite-fault models, which may be poorly resolved due to weak radiation of body waves. A comprehensive system that properly integrates seismic, tsunami, and geodetic measurements for the development of rapid earthquake rupture and tsunami excitation models would be a major improvement to providing timely and accurate tsunami forecasts for coastlines at risk from tsunami inundation. The development of robust tsunameter, geodetic, and seismic networks, communications, automated modeling, and decision-making procedures is essential.

6. Conclusions

Data collected from the 11 March 2011 earthquake and tsunami, including regional and global seismometers, GPS land stations, and deep-ocean tsunameters, are the earliest available observations useful for real-time or near-real-time tsunami source inversions. Measurements provided by these devices were used to estimate the earthquake and tsunami sources. In this study, we explore the near-field impact of the 11 March 2011 Japan tsunami via comparisons of three source models inferred from tsunameter measurements alone, from GPS and tsunami measurements combined, or from seismic waveforms. These source models are used as inputs to the MOST tsunami modeling software to simulate the generation, propagation, and inundation of the Japanese tsunami. Results permit comparative study to further understand the strengths and limitations of each modeling approach from the perspective of local tsunami predictions.

This study compares modeling results with deep-ocean and nearshore tsunami waveform observations, surveyed tsunami runup heights and inundation heights, and inundation limits and areas. Among the three source models, the tsunameter-derived real-time source, though an unexceptional characterization of the earthquake rupture geometry, presents the most complete agreement with tsunami observations, and in particular provides the best comparison with the high tsunami runup and inundation depths along the Sanriku Coast. The GPS/tsunameter and seismic source models perform well in the southern region (south of Sendai) of the earthquake rupture. The GPS/tsunameter source model underestimates by about 50 % the maximum runup of 30 to 40 m along the coastline between latitude 39°N and 40°N. The seismic source model predicts wave heights of just 10 m in the same location. A land-failure-induced disturbance in the northern rupture area, not captured by either the seismometer networks or the GPS stations, may explain the underestimation of tsunami runup in those models.

These model studies highlight the critical role of deep-ocean tsunami measurements—the earliest available tsunami data during the Japan event—for tsunami modeling and prediction. The source models generated using these measurements, such as the tsunameter-derived source model and the GPS/tsunameter-derived source model, have led to high-quality tsunami modeling results validated by real-time and posttsunami observations. Direct use of tsunami measurements in such source inversions reduces the ambiguity of the interaction between fault rupture and tsunami generation, and thus is the key for efficient and accurate tsunami forecasts. These direct tsunami measurements help to capture, in real time, the tsunami characteristics that are not directly related to the earthquake rupture and cannot be explained by available seismic data. Reducing the lag time between collection and availability and use of these measurements for near-field warning and inundation forecasts is an issue that should be addressed in the near future. GPS measurements, when made available more rapidly after an earthquake, and seismic models, when generated sooner without significantly sacrificing accuracy, would help reduce the lag time to create more effective assessment of the impending tsunami hazard in the near

field. However, we suggest that these data be combined with tsunami measurements to produce the best estimates of tsunami impact along near-field coastlines. Recent deployment of deep-ocean tsunameters offshore of Japan, between the trench and the coastline, has shortened the earliest direct tsunami observations and detection times to less than 20 min, depending on source location.

With the exception of a very few underwater observation points (e.g., SATO *et al.*, 2011), GPS devices are predominantly restricted to land areas. International scientific communities are now stressing the need for improved underwater deformation monitoring methods and increased data collection and access. This study shows that deep-ocean tsunami measurements are highly complementary to onland GPS for estimating the earthquake rupture area, leading to more complete understanding of both the earthquake source properties and the tsunami generation process. In the coming years, combining such GPS and tsunami geodetic data with seismic data (particularly where GPS and tsunameter data are scarce) may lead to the best early estimates of earthquake rupture and tsunami-generating processes useful for both real-time forecasting as well as early post-event disaster relief.

We also stress that the short-term forecasting of tsunamis described in this study is different from the long-term assessment of tsunami hazards, which prepares a coastal community for maximal probable tsunami scenarios. A long-term tsunami hazard assessment may include predicting future hazards based on available knowledge or some assumptions of the physical origin of a tsunami. It can also include the identification of new physical processes responsible for generating large tsunamis, and forecasting future events based on such new findings. It is worth noting that the methods and tools developed for short-term forecasts, such as those discussed in this paper, are very useful for helping to improve long-term tsunami hazard assessments. Both approaches need to be carried out, continuously and interactively, to better mitigate future tsunamis.

Acknowledgments

REFERENCES

ARCAS, D., and TITOV, V. (2006). *Sumatra tsunami: Lessons from modeling*, Surv. Geophys., *27*(6), doi:10.1007/s10712-006-9, 679–705.

BIRD, P. (2003). *An updated digital model of plate boundaries*, Geochem. Geophys. Geosys., *4*(3), 1027, doi:10.1029/2001GC000252.

BASSIN, C., LASKE, G. and MASTERS, G., (2000). *The current limits of resolution for surface wave tomography in North America*, EOS Trans. AGU, *81*, Fall Meet. Suppl., Abstract S12A-03.

BERNARD, E.N., TANG, L., WEI, Y., and TITOV, V.V. (2013). *Impact of near-field, deep-ocean tsunami observations on forecasting the December 7, 2012 Japanese tsunami*, submitted to this issue, in press (this issue), doi:10.1007/s00024-013-0720-8.

BLASER, L., KRÜUGER, F., OHRNBERGER, M. and SCHERBAUM, F., (2010). *Scaling relations of earthquake source parameter estimates with special focus on subduction environment*, Bull. Seismol. Soc. Am., *100*, 2914–2926.

BLEWITT, G., KREEMER, C., HAMMOND, W.C., PLAG, H.P., STEIN, S. and OKAL, E. (2006). *Rapid determination of earthquake magnitude using GPS for tsunami warning system*, Geophys. Res. Lett., *33*, L11309, doi:10.1029/2006GL026145.

BORRERO, J., BELL, R., CSATO, C., DELANGE, W., GREER, D., GORING, D., PICKETT, V. and POWER, W. (2013). *Observations, effects and real time assessment of the March 11, 2011 Tohoku-oki tsunami in New Zealand*, Pure Appl. Geophys., *170*, 1229–1248, doi:10.1007/s00024-012-0492-6.

BURWELL, D., TOLKOVA, E. and CHAWLA, A. (2007). *Diffusion and dispersion characterization of a numerical tsunami model*. Ocean Model., *19*(1–2), 10–30.

CHEN, T., NEWMAN, A.V., FENG, L., FRITZ, H.M. (2009). *Slip distribution from the 1 April 2007 Solomon Islands earthquake: a unique image of near-trench rupture*, Geophys. Res. Lett., *36*, L16307, doi:10.1029/2009GL039496.

CROWELL, B. BOCK, W.Y., MELGAR, D. (2012). *Real-time inversion of GPS data for finite fault modeling and rapid hazard assessment*, Geophys. Res. Lett., *39*(9), doi:10.1029/2012GL051318.

DUPUTEL, Z., RIVERA, L., KANAMORI, H., and HAYES, G. (2012). *W phase source inversion for moderate to large earthquakes (1990–2010)*, Geophys. J. Int. *189*, 1125–1147.

DZIEWONSKI, A,M. and ANDERSON, D.L., 1981. *Preliminary reference Earth model*, Phys. Earth Planet. Inter., *25*, 297–356.

FRITZ, H.M., BORRERO, J.C., SYNOLAKIS C.E., OKAL, E.A., WEISS, R., TITOV, V.V., JAFEE, B.E., FOTEINIS, S., LYNETT, P.K., CHAN, I-C., and LIU, P.L-F. (2011). *Insights on the 2009 South Pacific*

tsunami in Samoa and Tonga from field surveys and numerical simulations, Earth-Sci. Rev., *107*, 66–75.

GICA, E., SPILLANE, M., TITOV, V.V., CHAMBERLIN, C. and NEWMAN, J.C. (2008). *Development of the forecast propagation database for NOAA's Short-term Inundation Forecast for Tsunamis (SIFT)*, NOAA Tech. Memo. OAR PMEL-139, pp 89.

GONZÁLEZ, F.I., BERNARD, E.N., MEINIG, C., EBLE, M., MOFJELD, H.O., and STALIN, S. (2005). *The NTHMP tsunameter network*, Nat. Hazards, *35*(1), Special Issue, U.S. National Tsunami Hazard Mitigation Program, 2005, 25–39.

GOVERNMENT ACCOUNTABILITY OFFICE (2006), "U.S. Tsunami Preparedness — Federal and state partners collaborate to help communities reduce potential impacts, but significant challenges remain," Report to Congressional Committees and Senator Dianne Feinstein, United States Government Accountability Office, pp 60.

GRILLI, S.T., HARRIS, J.C., KIRBY, J.T., SHI, F., and MA, G., MASTERLARK, T., TAPPIN, D.R. and TAJALI-BAKHSH, T.S. (2013a). Modeling of the Tohoku-Oki 2011 tsunami generation, far-field and coastal impact: A mixed co-seismic and SMF source. In Proc. 7th Intl. Conf. on Coastal Dynamics (Arcachon, France, June 2013) (ed. P. Bonneton), 749–758, paper 068.

GRILLI, S.T., HARRIS, J.C., TAJALIBAKHSH, T., MASTERLARK, T.L., KYRIAKOPOULOS, C., KIRBY, J.T. and SHI, F. (2013b). *Numerical simulation of the 2011 Tohoku tsunami based on a new transient FEM co-seismic source: comparison to far- and near-field observations*. Pure Appl. Geophys., *170*, 1333–1359.

GUSMAN, A.R., TANIOKA, Y., KOBAYASHI, T., LATIEF, H. and PANDOW, W. (2010). *Slip distribution of the 2007 Bengkulu earthquake inferred from tsunami waveforms and InSAR data*, J. Geophys. Res., *115*, B12316, doi:10.1029/2010JB007565.

GUSMAN, A.R., TANIOKA, Y., SAKAI, S., TSUSHIMA, H. (2012). *Source model of the great 2011 Tohoku earthquake estimated from tsunami waveforms and crustal deformation data*. Earth Planet. Sci. Lett., *341–344*, 234–242.

HAYES, G.P. (2011). *Rapid source characterization of the 2011 Mw 9.0 off the Pacific Coast of Tohoku earthquake*, Earth Planets Space, *63*, 529–534.

HAYES, G.P., EARLE, P.S., BENZ, H.M., WALD, D.J., BRIGGS, R.W., and the USGS/NEIC Earthquake Response Team (2011). *88 Hours: The U.S. Geological Survey National Earthquake Information Center response to the 11 March 2011 Mw 9.0 Tohoku earthquake*, Seis. Res. Lett. *82*(4), 481–493.

HAYES, G.P., WALD, D.J., JOHNSON, R.L. (2012). *Slab 1.0: A three-dimensional model of global subduction zone geometries*, J. Geophys. Res.: Solid Earth, *117*, B01302, doi:10.1029/2011JB008524.

HIRATA, K., SATAKI, K., TANIOKA, Y., KURAGANO, T., HASEGAWA, Y., HAYASHI, Y., and HAMADA, N. (2006). *The 2004 Indian Ocean tsunami: Tsunami source model from satellite altimetry*, Earth Planets Space, *58*, 195–201.

JI, C., WALD, D.J., and HELMBERGER, D.V. (2002). *Source description of the 1999 Hector Mine, California earthquake; part I: wavelet domain inversion theory and resolution analysis*, Bull. Seismol. Soc. Am., *92*(4), 1192–1207.

JI, C., HELMBERGER, D.V., WALD, D.J. and MA, K.-F., 2003. *Slip history and dynamic implications of the 1999 Chi–Chi, Taiwan, earthquake*, J. Geophys. Res., *108*, doi:10.1029/2002JB001764.

KAJIURA, K., (1970). *Tsunami source, energy and the directivity of wave radiation*, Bull. Earthq. Res. Inst., Univ. Tokyo, *48*, 835–869.

KATO, T., TERADA, Y., KINOSHITA, M., KAKIMOTO, H., ISSHIKI, H., MATSUISHI, M., YOKOYAMA, A., and TANNO, T. (2000). *Real-time observation of tsunami by RTK-GPS*, Earth Planets Space, *52*, 841–845.

KATO, T., TERADA, Y., NAGAI, T., SHIMIZU, K., TOMITA, T. and KO-SHIMURA, S. (2008). Development of a new tsunami monitoring system using a GPS buoy, American Geophysical Union, Fall Meeting 2008, abstract #G43B-03.

LANGBEIN, J. and BOCK, Y (2004). *High-rate real-time GPS network at Parkfield: utility for detecting fault slip and seismic displacements*, Geophys. Res. Lett., *31*(15), doi:10.1029/2003GL019408.

LOVHOLT, F., PEDERSON, G. and GLIMSDAL, S. (2010). *Coupling of dispersive tsunami propagation and shallow water coastal response*. Open Oceanogr. J., *4*, 71–82.

MACINNES, B.T., GUSMAN, A.R., LEVEQUE, R.J., and TANIOKA, Y. (2013). *Comparison of earthquake source models for the 2011 Tohoku-oki event using tsunami simulations and near field observations*. Bull. Seismol. Soc. Am., *103*, no. 2B, 1256–1274, doi:10.1785/0120120121.

Ministry of Land, Infrastructure, Transport, and Tourism of Japan (2011a). Status survey reports of the East Japan Earthquake, Ministry of Land, Infrastructure, Transport, and Tourism Press Release (first report), pp 16.

Ministry of Land, Infrastructure, Transport, and Tourism of Japan (2011b). The Great East Japan Earthquake (107th report): Outline, Ministry of Land, Infrastructure, Transport, and Tourism, pp 1.

MORI, N., TAKAHASHI, T., YASUDA, T. and YANAGISAWA, H. (2011). *Survey of 2011 Tohoku earthquake tsunami inundation and run-up*, Geophys. Res. Lett., *38*, L00G14, doi:10.1029/2011GL049210.

NEWMAN, A.V. (2011). *Hidden depth*, Nature, *474*, 441–443.

NEWMAN, A.V., HAYES, G., WEI, Y. and CONVERS, J. (2011). *The 25 October 2010 Mentawai tsunami earthquake, from real-time discriminants, finite-fault rupture, and tsunami excitation*. Geophys. Res. Lett., *38*(5), L05302, doi:10.1029/2010GL046498.

OHTA, Y., KOBAYASHI, T., TSUSHIMA, H., MIURA, S., HINO, R., TAKASU, T., FUJIMOTO, H., IINUMA, T., TACHIBANA, K., DEMACHI, T., SATO, T., OHZONO, M., and UMINO, N. (2012), *Quasi real-time fault model estimation for near-field tsunami forecasting based on RTK-GPS analysis: application to the 2011 Tohoku-Oki earthquake (M_w 9.0)*, J. Geophys. Res. *117*, B02311, doi:10.1029/2011JB008750.

OKAL, E.A. and SYNOLAKIS, C.E. (2004). *Source discriminants for near-field tsunamis*, Geophys. J. Int., *158*, 899–912, doi:10.1111/j/1365-246X.2004.02347.x.

OKADA, M. (1985). *Surface deformation due to shear and tensile faults in a half-space*. Bull. Seismol. Soc. Am., *75*(4), 1135–1154.

OWEN, S.E., WEBB, F., SIMONS, M., ROSE, P.A., CRUZ, J., YUN, S., FIELDING, E.J., MOORE, A.W., HUA, H., and AGRAM, P.S. (2011). The ARIA-EQ project: Advanced Rapid Imaging and Analysis for Earthquakes, *American Geophysical Union*, Fall Meeting 2011, abstract #1N11B-1298.

OZAKI, T. (2012). *JMA's tsunami warning for the 2011 great Tohoku earthquake and tsunami warning improvement plan*. J. Disaster Res., *7*(7), 439–445.

PERCIVAL, D.B., DENBO, D.W., EBLE, M.C., GICA, E., MOFJELD, H.O., SPILLANE, M.C., TANG, L., and TITOV, V.V. (2010). *Extraction of tsunami source coefficients via inversion of DART® buoy data*, Nat. Hazards, doi:10.1007/s11069-010-9688-1.

Pietrzek, J., Socquet, A., Ham, D., Simons, W., Vigny, C., Labeur, R.J., Schrama, E., Stelling, G., and Vatvani, D. (2007). *Defining the source region of the Indian Ocean tsunami from GPS, altimeters, tide gauges and tsunami models*, Earth Planet. Sci. Lett., *261*(1–2), 49–64.

Rabak, I., Melbourne, T. I., Santillan, M., Scrivner, C.W., Kinkaid, K., Stahl, R., Rapid assessment and mitigation of Cascadia earthquakes using the combined PANGA and PBO real-time GPS networks, *Abstract G11C-04, presented at the 2010 Fall Meeting, AGU, San Francisco, Calif.,* 2010.

Rivera, L.A., Kanamori, H., and Duputel, Z. (2011). W phase source inversion using high-rate regional GPS data of the 2011 Tohoku-oki earthquake, *Abstract G33C-04 presented at the 2011 Fall Meeting, AGU, San Francisco, Calif., 5–9 Dec.*

Satake, K. (1987). *Inversion of tsunami waveforms for the estimation of a fault heterogeneity: Methods and numerical experiments*, J. Phys. Earth, *35*, 241–254.

Satake, K. and Kanamori, H. (1991). *Use of tsunami waveforms for earthquake source study*, Nat. Hazards, *4*, 193–208.

Sato, M., Ishikawa, T., Ujihara, N., Yoshida, S., Fujita, M., Mochizuki, M., and Asada, A. (2011). *Displacement above the hypocenter of the 2011 Tohoku-Oki earthquake*, Science, *332*(6036), 1395, doi:10.1126/science.1207401.

Simons, M., Minson, S.E., Sladen, A., Ortega, F., Jiang, J., Owen, S.E., Meng, L., J-P. Ampuero, S. Wei, R. Chu, D.V. Helmberger, H. Kanamori, E. Hetland, A.W. Moore, and F.H. Webb (2011), *The 2011 magnitude 9.0 Tohoku-Oki earthquake: Mosaicking the megathrust from seconds to centuries*, Science, *332*(6036), 2011, pp. 1421–1425.

Song, Y.T., Fukumori, I., Shum, C.K., and Yi, Y. (2012). *Merging tsunamis of the 2011 Tohoku-Oki earthquake detected over the open ocean*. Geophys. Res. Lett., *39*, L05606, doi:10.1029/2011GL050767.

Spillane, M.C., Gica, E., Titov, V.V., and Mofjeld, H.O. (2008) *Tsunameter network design for the U.S. DART® arrays in the Pacific and Atlantic Oceans*, NOAA Tech. Memo. OAR PMEL-143, pp 165.

Synolakis, C.E., Bernard, E.N., Titov, V.V., Kânoğlu, U., and González, F.I. (2008). *Validation and verification of tsunami numerical models*, Pure Appl. Geophys., *165*(11–12), 2197–2228.

Tang, L., Titov, V.V., Bernard, E.N., Wei, Y., Chamberlin, C., Newman, J.C., Mofjeld, H., Arcas, D., Eble, M., Moore, C., Uslu, B., Pells, C., Spillane, M.C., Wright, L.M., and Gica, E. (2012). *Direct energy estimation of the 2011 Japan tsunami using deep-ocean pressure measurements.* J. Geophys. Res., *117*, C08008, doi:10.1029/2011JC007635.

Tang, L., Titov, V.V., and Chamberlin, C.D. (2009). *Development, testing, and applications of site-specific tsunami inundation models for real-time forecasting*, J. Geophys. Res., *114*, C12025, doi:10.1029/2009JC005476.

Tang, L., Titov, V.V., Wei, Y., Mofjeld, H.O., Spillane, M., Arcas, D., Bernard, E.N., Chamberlin, C., Gica, E., and Newman, J. (2008). *Tsunami forecast analysis for the May 2006 Tonga tsunami*, J. Geophys. Res., *113*, C12015, doi:10.1029/2008JC004922.

Titov, V.V. (2009). Tsunami forecasting, Chapter 12 in *The Sea, Volume 15: Tsunamis*, Harvard University Press, Cambridge, MA and London, England, 371–400.

Titov, V., and González, F.I. (1997). Implementation and testing of the Method of Splitting Tsunami (MOST) model, *NOAA Tech. Memo. ERL PMEL-112 (PB98-122773)*, NOAA/Pacific Marine Environmental Laboratory, Seattle, WA, 11 pp.

Titov, V.V., González, F.I., Bernard, E.N., Eble, M.C., Mofjeld, H.O., Newman, J.C., and Venturato, A.J. (2005). *Real-time tsunami forecasting: challenges and solutions*, Nat. Hazards, *35*(1), Special Issue, U.S. National Tsunami Hazard Mitigation Program, 41–58.

Titov, V.V., and Synolakis, C.E. (1998). *Numerical modeling of tidal wave runup*, J. Waterw. Port Coastal Ocean Eng., *124*(4), 157–171.

Tsushima, H., Hino, R., Fujimoto, H., Tanioka, Y., and Imamura, F. (2009). *Near-field tsunami forecasting from cabled ocean bottom pressure data*, J. Geophys. Res., *114*, B06309, doi:10.1029/2008JB005988.

Vigny, C., Socquet, A., Peyrat, S., Ruegg, J.C., Métois, M., Madariaga, R., Morvan, S., Lancieri, M., Lacassin, R., Campos, J., Carrizo, D., Bejar-Pizarro, M., Barrientos, S., Armijo, R., Aranda, C., Valderas-Bermejo, M.C., Ortega, I., Bondoux, F., Baize, S., Lyon-Caen, H., Pavez, A., Vilotte, J.P., Bevis, M., Brooks, B., Smalley, R., Parra, H., Baez, J.C., Blanco, M., Cimbaro, S., Kendrick, E. (2011). *The 2010 Mw 8.8 Maule megathrust earthquake of central Chile, monitored by GPS*, Science, 332, 1417–1421.

Wang, X. and Liu, P.L.-F. (2007), *Numerical simulations of the 2004 Indian Ocean tsunamis—coastal effects*, J. Earthq. Tsunami, *1*(3), 273, doi:10.1142/S179343110700016X.

Wei, Y., Bernard, E., Tang, L., Weiss, R., Titov, V.V., Moore, C., Spillane, M., Hopkins, M.,.and Kânoğlu, U. (2008). *Real-time experimental forecast of the Peruvian tsunami of August 2007 for U.S. coastlines*, Geophys. Res. Lett., *35*, L04609, doi:10.1029/2007GL032250.

Wei, Y., Chamberlin, C., Titov, V.V., Tang, L. and Bernard, E.N. (2013). *Modeling of the 2011 Japan tsunami: Lessons for near-field forecast*, Pure Appl. Geophys., *170*, 1309–1331.

Wei, Y., Cheung, K.F., Curtis, G.D., and McCreery, C.S. (2003). *Inversion algorithm for tsunami forecast*, J. Waterw. Port Coastal Ocean Eng., *129*, 2003, pp. 60–69.

Whitmore, P.M. (2009). Tsunami warning systems, Chapter 13 in *The Sea, Volume 15: Tsunamis*, Harvard University Press, Cambridge, MA and London, England, 401–442.

Yamazaki, Y., Lay, T., Cheung, K.F., Yue, H., and Kanamori, H. (2011). *Modeling near-field tsunami observations to improve finite-fault slip models for the 11 March 2011 Tohoku earthquake*. Geophys. Res. Lett., *38*(7), doi:10.1029/2011GL049130.

Yokota, Y., Koketsu, K., Fujii, Y., Satake, K., Sakao, S., Shinohara, M., and Kanazawa, T. (2011). *Joint inversion of strong motion, teleseismic, geodetic, and tsunami datasets for the rupture process of the 2011 Tohoku earthquake*, Geophys. Res. Lett., 38, L00G21, doi:10.1029/2011GL050098.

Yue, H., Lay, T., Schwartz, S. Y., Rivera, J., Protti, M., Dixon, T., Owen, S., Newman, A. (2013). *The 5 September 2012 Nicoya, Costa Rica Mw 7.6 earthquake rupture process from joint inversion of high-rate GPS, strong-motion, and teleseismic P wave data and its relationship to adjacent plate boundary interface properties*, J. Geophys. Res. Solid Earth, *118*(10), 5453–5466.

Zhou, H., Moore, C., Wei, Y.and Titov, V.V. (2011). *A nested-grid Boussinesq-type approach to modeling dispersive propagation*

and runup of landslide-generated tsunami. Nat. Hazards Earth Syst. Sci., *11*(10), 2677–2697, doi:10.5194/nhess-11-2677-2011.

ZHOU, H., WEI, Y., WRIGHT, L., and TITOV, V.V (2014). *Waves and currents in Hawaii waters induced by the dispersive 2011 Tohoku tsunami*. Pure Appl. Geophys., doi:10.1007/s00024-014-0781-3

ZHOU, H., WEI, Y., and TITOV, V.V. (2012). *Dispersive modeling of the 2009 Samoa tsunami*. Geophys. Res. Lett., *39*(16), L16603, doi:10.1029/2012GL053068.